Evaluation of New Radar Technologies

OPERA-3 Deliverable OPERA_2012_04

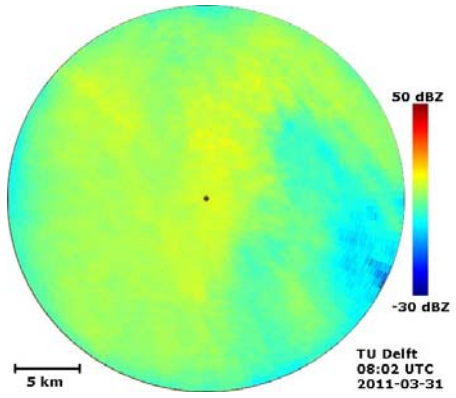

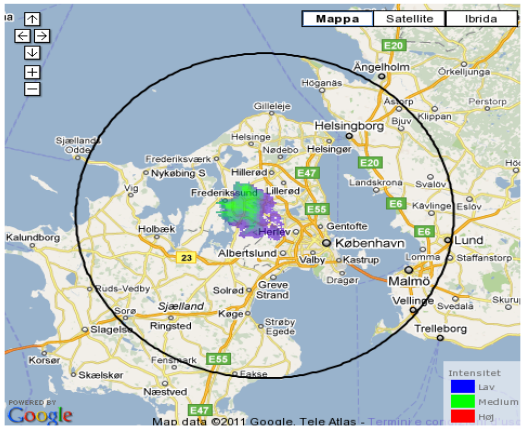

Lead: ARPA Piemonte (*R. Cremonini*)

Contributors: Météo France (*P. Tabary*), UK Met Office (*J. Sugier*), DWD (*M. Frech*), ARPA Emilia Romagna (*P.P. Alberoni*), CNR (*L. Baldini*)

April, 2012

Project summary

General Informations	
Project Title	**E-NRadTech**
Acronym	**E**valuation of **N**ew **Rad**ar **Tech**nologies
Starting date	1-Jan-2010
Duration	24 months
Call identifier	OPERA – 3 Deliverable OPERA_2012_04
Keywords	Polarimetric radars, X-band radar, multiparamter rainfall estimation, data quality, maintenance and radome issue, hydrometeor classification
Description	The aim of the project is evaluating the new operational radar technologies focusing on the operational use of polarimetric weather radars at C, S and X-band. Special emphasis will be laid on X-band operational, economic and scientific aspects will be covered. An evaluation of extended capabilities of signal processors and scanning schema of C-band operational radar in comparison with X-band radar will be also carried out, assessing advantages and drawbacks towards radar data quality.

Project team

	Partner	Acronym	Country	Reference
1	Météo France	MF	FRANCE	Pierre Tabary
2	UK Met Office	UKMET	UK	Jacqueline Sugier
3	DWD	DWD	GERMANY	Michael Frech
4	ARPA Piemonte	ARPAP	ITALY	Roberto Cremonini
5	ARPA Emilia Romagna	ARPA-EMR	ITALY	Pier Paolo Alberoni
6	CNR-ISAC	CNR	ITALY	Luca Baldini

Table of contents

Introduction

This work has the essentially two main objectives:

- To provide OPERA members with an operational overview on emerging technologies and algorithms so that they can make the right decision regarding the upgrade of their networks and their investment in R&D activities.

- To provide a platform for exchanging and reporting technical and scientific advancement within the OPERA community in order to foster innovation as well as standardization.

In complex terrain the radar beam can experience partial or total blocking. As a consequence, in regions characterized by a complex orography, the coverage of operational C-band networks is often inadequate or even non-existent. This problem often occurs in Europe. This problem can be partially mitigated by resorting to sampling precipitation at higher elevation, causing decorrelation between precipitation estimates by radar and rainfall measured at ground. Coverage gaps typically occur in mountainous basins. X-band radars can offer a viable solution to fill gaps of these networks in mountainous regions. Nowadays X-band radars represent a cost- effective solution because these radars are much cheaper (in direct cost, infrastructure and maintenance costs) than traditional C-band or S-band radars with the same beamwidth. Their main disadvantage is represented by the attenuation due to propagation through precipitation that determines important errors in radar rainfall estimation obtained from parameters derived from power measurements. The use of dual-polarization techniques in X-band radar systems has provided solutions to mitigate the impact of attenuation. This fact has revived in the recent years the interest of the scientific and the operational communities about X-band radar; these systems are now considered a convenient solution for applications such as rainfall monitoring over a small watershed, to fill gaps in operational radar network and for improving lower atmosphere coverage, and capability to trace and track storm cells in the presence of small scale and high impact cases. An important aspect related to the reduced size of X-band systems is the possibility of implementing them as mobile system. In this way they can be quickly deployed and used to provide adequate coverage of specific areas subjected to emergencies. Among advantages of X-band for dual polarization radar systems we can mention the improved sensitivity of differential phase measurements to precipitation. This sensitivity allows

building up reliable algorithms for rainfall estimation based on the use of differential phase shift, a parameter based on phase of radar return, immune to attenuation caused by propagation and by beam blocking (Wang and Chandrasekar 2009). This feature increase usefulness of X-band polarimetric systems in estimating precipitation in mountainous area.

However, the use of X-band radars as part of networks (such as gap filler for C-band national networks) rather than as stand-alone systems requires specific investigations, ranging from the study of specific topics on X-band systems and related precipitation estimation algorithms and networking methodologies as well. On the other hand, plans to upgrade operational C-band radars to polarimetry are ongoing almost in every country and specific issues concerning networking of heterogeneous polarimetric systems operating with different polarimetric configurations, different signal processing and affected in a different way by error sources need to be considered.

Several new installations of X-band polarimetric radar exists worldwide and in Europe. Although mostly pre-operational, they are acquiring data with adequate continuity.

Different systems have been tested during several EU-funded or National projects focused on operational systems:

- FRAMEA project, Alcotra programme 2003 – 2007, tested polarimetric Doppler X-band radar in Alpine regions;
- ForeAlps project, Alcotra programme 2003 – 2007, also tested low-cost X-band microradar;

In the US, the project CASA (Center for Collaborative Adaptive Sensing of the Atmosphere; (Mc Laughlin at al. 2009) aims to deploy an experimental network of small X band polarimetric radars in Oklahoma as a proof of concept of a new paradigm for precipitation sensing based on low cost X-band polarimetric radar with overlapping coverage;

In Japan, the NIED (National Research Institute for Earth Science and Disaster Prevention) deployed an experimental network of three X band polarimetric radars (X-NET) in the Tokyo metropolitan area to improve the coverage of the regular C-band radar network of the Japan Meteo Agency (Maesaka et al. 2011).

Although the use of X-band radars is increasing and successfully demonstrated for many applications, there are several applications, such that of gap filler, that still need systematic study of using X-band radar in cooperation with C-band operational radar network focusing on mountain regions.

Survey of existing X-band radar in Europe

(Leader : ARPA Piemonte; Contributors : ARPA EMR, CNR, Météo France)

There is a growing interest in X band polarimetric systems. Systems with different characteristics and prices are available from several manufacturers. The number of installations and projects targeting different applications of X-band radar is rapidly growing as well.

During the past year an extensive survey of existing X-band systems has been performed, considering operational, pre-operational or research X-band radar used in Europe for local purposes or as complement of C-band radar networks. The current survey includes only horizontally or volumetric scanning radar (i.e. vertical pointing radar are excluded) managed by meteorological, hydrological or research institutes. Moreover, both non polarimetric and dual polarization systems have been analyzed.

Figure 1 X-band radar installed in Davos (CH)

The *Annex 1* reports complete results updated on March 2011. OPERA 3 - WP1.4b aims at to maintain a database of the ongoing projects that include the development or the deployment of X-band radars.

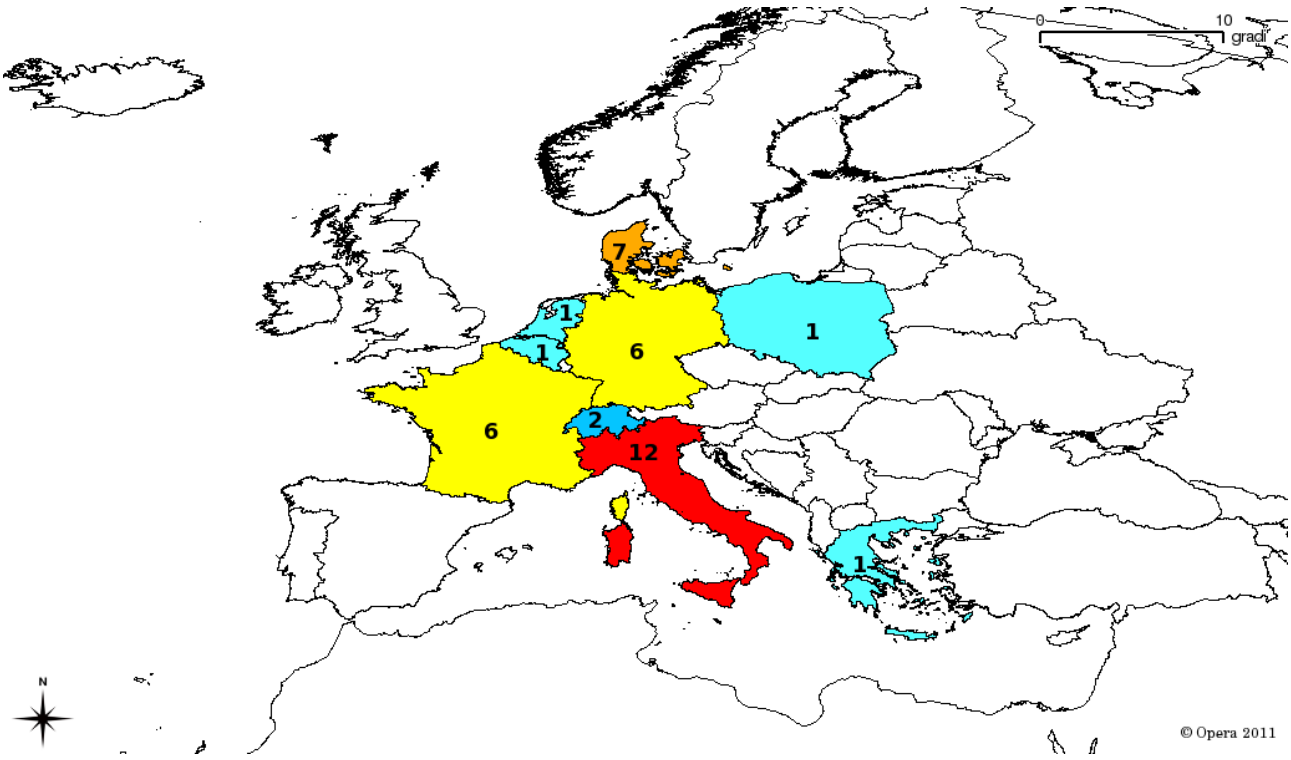

Fig 2: X-band radar in Europe at March 2011

The figure 2 shows the distribution of X-band radars by country updated at March 2011. Italy and Denmark are the country where X-band technologies have grown more during past years, followed by France and Germany. Meanwhile in Denmark there is a homogeneous network of Doppler small radar, mainly focused on local weather. In Italy, and also in France and Germany, different type of instruments are installed in different regions. About 33% of overall installations are polarimetric with radome, while 15 radar remaining are non-Doppler and non-polarimetric radars. Notable for technology development is the Delft FMCW research radar in Delft (NL). The declared maximum useful range varies from 40 km to 100 km, showing quite widespread values between different systems.

Regarding the antenna, some radars exhibit a fan-beam antenna with horizontal resolution of 0.95° and vertical one 20°. Others, using a standard parabolic reflector, declare horizontal and vertical resolution ranging from 1.35° to 4°. Highest installations are located in Swiss, on Klein Matterhorn (Zermatt) at 3,888 m a.s.l. and in Davos at 2,152 m a.s.l.

These new installations are sometimes mobile and related to the support of emergency operations due to natural phenomena allowing radar monitoring, like volcanic ashes (Italy). More frequently, installations are related to research, local or municipality weather services (Denmark, Mt.Vial in

France), gap filling (France) or Alpine hydrology (Swiss).

Although few information has been collected, X-band costs costs seem to range from 50 kEuro to 500-700 kEuro, depending on systems characteristics, such as polarimetry. Only Swiss and Belgium provided rough maintenance costs. One possible interpretation could be related to the young age of the installations and maintenance problems will be faced during next years.

In spite of the growth of the number of projects employing X-band radars, both as standalone or networked system, an aspect that should be more carefully considered is how or if these new instruments are planned to be integrated with other operational measurements like raingauge ground networks and operational C-band Radar. At the moment, only one X-band radar is delivered operationally to the Opera composite by Italy; soon with the ongoing French RHYTMME project new radars will be included.

Preliminary X-band assessment on data quality

Some result on X-band assessment on data quality come from Arpa Piemonte and MétéoFrance experiences.

Thorough investigations on radome effects have been performed by Frech et al. (2099) using one year of measurements collected by a 12 year old orange-peel radome that was not properly maintained (see Annex 1 for details).

As reported by Annex 2, aspects related to relatively new radome (less than 2 year old) impacts have been also investigated by Arpa Piemonte in collaboration with the Colorado State University (Bechini et al. 2010). An experiment was conducted using the X-band dual-polarization radar of ARPA Piemonte and a laser disdrometer (http://www.thiesclima.com/disdrometer.html), installed besides the ARX radar trailer. The disdrometer provides particle counts in 22 classes of diameters (0.16 mm to > 8 mm) and 20 classes of velocity (0.2 m/s to 20 m/s). The measured Drop Size Distribution (DSD) is used to retrieve both the rainfall rate and the horizontal radar reflectivity Zh. Although the deviation from Raileigh scattering is in general small for the light to moderate rainfall intensities considered (Zh < 45 dBZ) the reflectivity is calculated using a T-matrix code (Waterman, 1979), in order to take into account possible Mie scattering effects at X-band. The rough linearity of the loss with $R^{1/3}$, derived during the experiment over the whole rain rate dynamics (0.05 to 25 mm/h) can be interpreted as an indication of the wetting radome surface (water film formation). In presence of a non wetting radome a sharp transition would be expected corresponding to the change in the water flow from rivulets to laminar. The radome was two years old at the time of these measurements and likely had lost the non wetting original conditions, due to degradation with time. Anderson (1975) has shown how this kind of degradation may occur after approximately 6 months (a loss increase from 0.5 to 7 dB over such time period is reported at 20 GHz). The radome, although originally declared hydrophobic by the manufacturer, clearly lost its hydrophobicity properties with time. This degradation may actually occur over a relatively short period of operation, e.g. several months (Anderson, 1975). In a perspective of a dense X-band radar network, a periodical polishing of the radome surface does not appear practical. So, only two options appear viable:

- **to operate the radar without the radome** (easier at X-band, due to the reduced dimensions, but still impractical in general for the higher wear and also for the “psychological”

impact of a scanning antenna);

- **to adopt a procedure to correct for attenuation effects in real time**. The results of this work provide some clue for the implementation of such correction.

The effects of non uniform radome wetting with azimuth and elevation (Bechini et al., 2006), e.g. due to wind direction, will also have to be considered for the implementation of a real-time correction procedure.

Météo France has presented (see Annex 3 for details) the current status of development of a polarimetric radar network data processing chain to provide accurate QPE to decision makers in a flooding-prone mountainous region. Results of preliminary tests on several Pol-QPE algorithms, based on simple Z-R relationships and on K_{dp}, have been summarized. K_{dp} has shown to be a very good candidate because it is insensitive to calibration errors and partial beam blocking. A synthetic Z-K_{dp} algorithm, which combines R-K_{dp} relations for intense precipitation and Z-R relations corrected for attenuation in the weak rain, has been tested and the one which shows the best score is achieved by a combined algorithm (Kabeche et al. 2011)

The next step will be to enhance the evaluation including more events and testing other polarimetric precipitation estimation algorithms, such as the integrated ZZDR technique by Illingworth & Thompson (2005), the variational approach (Hogan, 2007) and ZPHI (Testud et al. 2000).

Once the optimal polarimetric precipitation estimating algorithm will be determined, the implementation of intelligent compositing rules between X-band radars have to be studied, allowing for a mitigation of attenuation effects and optimal exploitation of the network. Maps of minimum detectable signal will also be produced and used in the compositing rules in order to mitigate situations of severe attenuation/extinction leading to complete misses of precipitation detection by radar.

Finally, as among Mt. Maurielle and Mt. Vial radars, one has a radome and the other one does not, new perspectives will be studied in the quantitative evaluation of wet radome attenuation on polarimetric measurements.

Recommendations for QPE with X-band radar

Results of the survey conducted in Europe have shown the common adoption of X-band radars for a number of meteorological and hydrological applications. However, different system characteristics correspond to different applications. Some examples of X-band radars are unique installations for research purposes. In spite of the different radars encounteres, it seems that for QPE applications some common solutions have been adopted; so that it is possible to outline recommendations concerning X-band radars for QPE applications.

Polarimetry

Power measurements at X-band, such as reflectivity factor, are affected by attenuation due to wave propagation through precipitation, even in case of weak precipitation. Studies have shown that iterative methods for reflectivity correction can diverge. Dual polarization radar measurements, in particular differential phase, give chances to mitigate attenuation problems, both estimating attenuation effects in reflectivity or to estimate precipitation intensity in algorithms using differential phase shift that can mitigate impact of drop size distribution variability. Nowadays most of dual polarization radars employ the STAR (simultaneous transmit and receive) scheme that allow reliable estimation of differential phase shift, although presents disadvantages in the differential estimation of differential reflectivity.

Antenna resolution

X-band systems allow smaller size antenna antennas with respect to an S- and C- band systems having the same resolution. However, X-band systems with poor horizontal or vertical resolution can present a limitation in the effective range that can be used for QPE. Recommendations for resolution can be different in azimuth and in elevation. In azimuth, at a 30-km distance, an azimuth resolution of 2° corresponds to a width of resolution cell of 1 km. Along the horizontal, this can be acceptable for obtaining rainfall maps with a 1-km resolution, but in vertical the same resolution could not be sufficient to assure quality differential phase shift measurements that are affected by vertical gradients, such as those collected in areas with partial contamination with the melting layer.

Radome

Many practical issues (cost limitation of the servo/antenna system, security of operations and protection from severe environmental conditions) suggest to install radome on radar systems to obtain measurements in conditions, such as intense wind gusts, that could hamper the functioning of an antenna non protected by the radome. However, several studies have shown its negative impacts on reflectivity and dual-polarization data quality. Performance of a radome depends on several

factors, such as the shape of the radome, actual hydrofobicity of the coating and its size. It has been shown that at X-band, loss due to radome wetting can reach the order of 10 dB in the case of heavy precipitation that is hard to estimate in real time. So it could be preferable operate without radome, provided that radar design adopts proper measures to ensure that antenna can withstand wind gusts and cooling of the systems obtained without the thermal insulation provided by the radome. Anyway, when radome is present, efforts must be spent to devise robust algorithms for reducing radome impact on measurements by operational attenuation corrections using phase measurements, or attenuation estimations derived from co-located disdrometer or by deriving QPE from differential phase measurements that seems less affectedby radome effects.

Receiver

State-of the art digital receiver should be used. They allow low noise figure (of the order of a few dBs) and linear response of at least 90 dB.

Transmitter

In dual polarization operational weather radars,, magnetron transmitter are commonly adopted. To define peak power several factors should be taken into accounts. In weather radars it is customary to define sensitivity based on the minimum detectable reflectivity factor at a given where the signal-to-noise ratio at a reference plan is 0 dB. Minimum detectable signal, receiver bandwidth /range resolution and transmitter duty cycle limitation are jointly related and are selected based on a minimum reflectivity detectable at a given distance. In the case of attenuating frequencies, a further margin, statistically determined to ensure that a signal be detectable at a given distance in condition of precipitation induced attenuation should be considered. A further margin to be taken into account is related to the attenuation induced by a wet radome.

Additional features:

The radar system should feature BITE remote control and online calibration tests. Moreover, a solar scan utility should be available for pointing and absolute calibration purposes.

References

Anderson, I., 1975: Measurements of 20-GHz transmission through a radome in rain. *IEEE Transactions on Antennas and Propagation*, vol. 23, no. 5, 619-622.

Bechini, R., R. Cremonini, E. Gorgucci and L. Baldini, 2006: Dual-pol radar calibration and correction of the bias introduced by non uniform radome wetting. *Proceedings, 4th European Conf. on Radar in Meteorology, Barcelona, Spain, ERAD*, 593-596.

Bechini, R., V.Chandrasekar, R. Cremonini, S. Lim, 2010: Radome attenuation at X-band radar operations. *Proc of the European Conference on radar Meterol and Hydrol ERAD 2010*

Frech M., The effect of a wet radome on dualpol data quality, *AMS Radar Conference, 2009*

Hogan, R.J., 2007: A Variational Scheme for Retrieving Rainfall Rate and Hail Reflectivity Fraction from Polarization Radar. *J. Appl. Meteor.*, Vol. 46, 1544-1563.

Kabeche F., J. Figueras i Ventura, B. Fradon, A. A. Boumahmoud, P. Dupuy, S. Westrelin, and P. Tabary , Quantitative Precipitation Estimation in the French Alps with a dense network of polarimetric X-band radars. 35th AMS Int. Conf. on Radar Meteorology, Pittsburgh PA.

Maesaka T. , M. Maki, K. Iwanami, S. Tsuchiya, K. Kieda, and A. Hoshi, 2011: Operational Rainfall Estimation by X-band MP Radar Network in MLIT, Japan, *Proc of 35th AMS Int. Conf. on Radar Meteorology*, Pittsburgh PA.

McLaughlin D, et al., 2009: , Short-wavelength technology and the potential for distributed networks of small radar systems, *Bull. of the American Meteorol. soc.*, 90 pp. 1797-1817.

Testud, J., Le Bouar E., Obligis E., and Ali-Mehenni M., 2000: The rain profiling algorithm applied to polarimetric weather radar, *J. Atmos. Oceanic Technol*., Vol. 17, 332-356

Wang, Y., V. Chandrasekar, 2010: Quantitative Precipitation Estimation in the CASA X-band Dual-Polarization Radar Network. *J. Atmos. Oceanic Technol.*, 27, 1665–1676.

Waterman P.C., 1979. Matrix methods in potential theory and electromagnetic scattering. *J. Appl. Phys.*, v.50, p.4550-4565.

Annex 1 - Radome impact on X-band measurements: ARPA Piemonte experience.

Aspects related to radome impacts has been investigated by Arpa Piemote in collaboration with Colorado State University.

A laser disdrometer (http://www.thiesclima.com/disdrometer.html) has been installed besides the ARX radar trailer. The disdrometer provides particle counts in 22 classes of diameters (0.16 mm to > 8 mm) and 20 classes of velocity (0.2 m/s to 20 m/s). The measured Drop Size Distribution (DSD) was used to retrieve both the rainfall rate and the horizontal radar reflectivity Zh. Although the deviation from Raileigh scattering is in general small for the light to moderate rainfall intensities considered (Zh < 45 dBZ) the reflectivity is calculated using a T-matrix code (Waterman, 1979), in order to take into account possible Mie scattering effects at X-band.

The first valid range for the ARX radar (considering the far-field, delays in the system and near clutter) is 800 m; using a gate spacing of 125 m, this corresponds to the 7th range bin. The lack of closer measurements prevents a direct comparison with the disdrometer, which is located just several meters from the radar trailer. Therefore, in order to compare the measurements of the two sensors, the following data selection procedure has been applied:

- select all measurements (0- 360 deg azimuth) at gate 7, for every elevation scan;
- calculate the mean (<Zh>) and standard deviation (σ(Zh)) for the obtained distribution, for every elevation;
- If σ (Zh) < 3 dB retain the data for the given time and elevation;
- compare with 5 minute average disdrometer reflectivity and calculate the bias:

$$bias\ (dB) = Zh_{radar}\ (dBZ) - Zh_{disdro}\ (dBZ) \qquad (1)$$

The condition on the standard deviation of *Zh* ensures that the precipitation is relatively uniform around the radar site. In fact, if the variability of the reflectivity on the circle with radius 800 m is low, then we may reasonably expect a similar (within the observed standard deviation) intensity all

over the area enclosed by the circle, including the radar. Under the same assumption of uniform precipitation field, the X-band path attenuation is calculated from the disdrometer DSD and used to correct the radar reflectivity on the circle. Eight precipitation events are considered between March and April 2009. After applying the above conditions, the maximum reflectivity was about 45 dBZ, a value that allows to exclude possible hail contamination.

The values of the bias in (1) are calculated for every precipitation event, for every elevation and for several classes of rain rate (calculated from the disdrometer DSD): 0.05, 0.2, 0.6, 2.0, 5.0, 12.0, 25.0 mm/h.

It is known that the radome attenuation mainly depends on the thickness of the water film flowing on its surface, which in turn is a function of the rain rate (Anderson, 1975). Therefore we look for an experimental power law relation to express the one-way power loss due to the wet radome as a function of the rain rate R (mm/h):

$$L_{radome}\,(dB) = -bias/2 \cdot = L_0 + a \cdot R^b \qquad (2)$$

where the factor of two in the bias takes into account the fact that the measured bias results from the two-way (transmit and receive) propagation through the radome. A non zero L_0 may arise from the existence of a threshold under which the radome attenuation becomes negligible and consequently the validity of (2) would be limited to values above a given rain rate. In fact at low rain rates a water film may not form under light precipitation, with consequent very low expected attenuation.

In order to find the coefficients a and b in (2), a linear regression with a varying coefficient b is performed until the Mean Square Error (MSE) is minimized. The MSE reaches a minimum for b~0.3 (fig. 1). According to the Gibble's formula (Gibble, 1964) for laminar flow, the water layer thickness is proportional to R1/3, for a hemispherical radome. The fit to eq. (2) with b = 1/3 (fig. 2) actually shows that the observed power loss is roughly proportional to $R^{1/3}$, i.e. to the theoretical water film thickness.

The obtained coefficients for the fit in fig. 2 (b = 1/3) are a = 1.75 and L_0 = -0.34 dB. Substituting into eq (2):

$$L_{radome}\ (dB) \sim -0.34 + 1.75 \cdot R^{1/3} \qquad 0.05 < R < 25\ mm/h \qquad (3)$$

Exploiting the dependence on the radome radius in the Gibble's formula, the above experimental formula can be generalized for application to different radome sizes:

$$L_{radome}\ (dB) \sim -0.34 + 1.61 \cdot (r \cdot R)^{1/3}; \qquad 0.05 < R < 25\ mm/h \qquad (4)$$

where r is the radius of the radome in m and R is the rain rate in mm/h.

The rough linearity of the loss with $R^{1/3}$ over the whole rain rate dynamics (0.05 to 25 mm/h) in fig. 2 can be interpreted as an indication of the wetting radome surface (water film formation). In presence of a non wetting radome a sharp transition would be expected corresponding to the change in the water flow from rivulets to laminar. The radome was two years old at the time of these measurements and likely had lost the non wetting original conditions, due to degradation with time. Anderson (1975) has shown how this kind of degradation may occur after approximately 6 months (a loss increase from 0.5 to 7 dB over such time period is reported at 20 GHz).

The presented experimental results can be compared with some theoretical and laboratory studies. The 4.5 dB loss at 25 mm/h found here roughly agrees with the ~4 dB loss at 10 GHz for a 0.1 mm water thickness (corresponding to 23 mm/h for a radome with 2.55 m diameter) found both in Effenberger et al. (1986) and in Chang (1986).

Kurri and Huuskonen (2008) measured the radome transmission loss for a 6.7 m radome at C-band. From fig. 2 in their paper, the loss at 10 °C water temperature can be approximated by $L_{radome}\ (dB) = 1.0\ R^{1/3}$, between 1 and 30 mm/h. Eq (3) then provides a rough estimate of a +75% wet radome attenuation at X-band compared to C-band, for typical radome sizes.

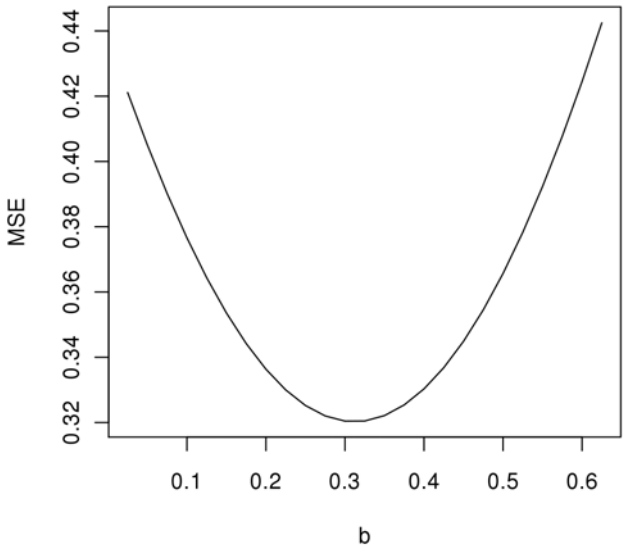

Figure 1. Mean Square Error (MSE) as a function of the exponent b in the power law relation (2).

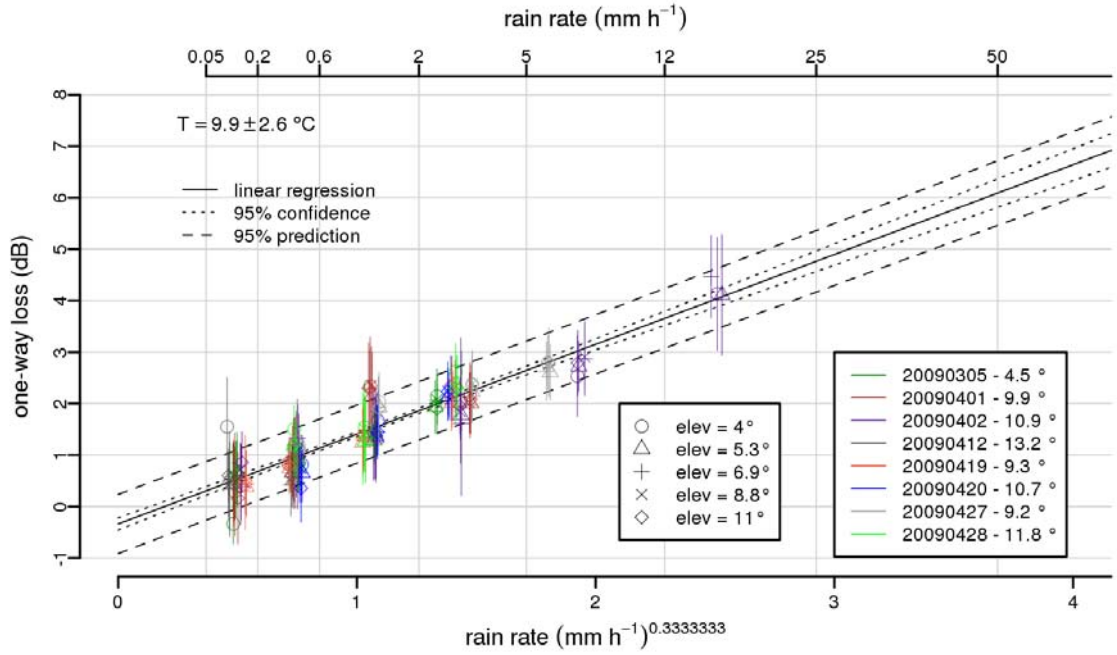

Figure 2. One-way loss (dB) as a function of the rain rate, using eq. (2), with b = 1/3. The right legend shows the date of the events with the corresponding air temperature in °C. The vertical bars represent the standard deviation of the loss, calculated over all measurements available within a given rain rate class.

In July 2009 a metal sphere calibration was performed on the X-band radar. The 30 cm diameter metal sphere was suspended at about 200 m AGL at 2 km distance from the radar. The measured gain of the system (~41.5 dB, including the antenna gain and tx + rx waveguide losses) compared well (within 0.5 dB) with the calculated value used in the system radar constant. After completing the normal sphere calibration, an irrigation sprinkler has been used to wet the radome surface while still collecting measurements with the antenna pointing at the suspended metal sphere. Fig. 3 (right) shows the measured gain during the experiment: the first 30 minutes correspond to measurements with the dry radome, the following 20 minutes with the wet radome; around 09:20 the sprinkler was closed and the gain started to raise again while the radome dried off.

The average intensity of the artificial rain, independently measured both with the laser disdrometer and a rain-gauge, was 156 ± 58 mm/h. The uncertainty on the artificial rain intensity is quite high due to the relatively small size of the sprinkler and the wind slightly changing the orientation of the irrigated water. The corresponding observed one-way loss is 6.5 ± 0.4 dB, which results in about 12-14 dB two-way attenuation.

Eq (4) for the 156 mm/h rainfall intensity would give 9 dB one-way loss, a value considerably higher than 6.4 dB. Actually the loss can only be approximated as a linear function of the water film for a relatively small thickness (Anderson, 1975), e.g. 0.1 mm, corresponding to about 20 mm/h for the given radome size). For 0.2 mm water thickness (~150 mm/h), Effenberger et al. (1986) reports a transmission loss in the 6.5-7.0 dB range, and Chang (1986) a value close to 6 dB, in good agreement with our observations.

In order to fill-in the experimental curve between 20 and 200 mm/h a better sprinkler is needed, including the possibility to adapt more accurately the water flow.

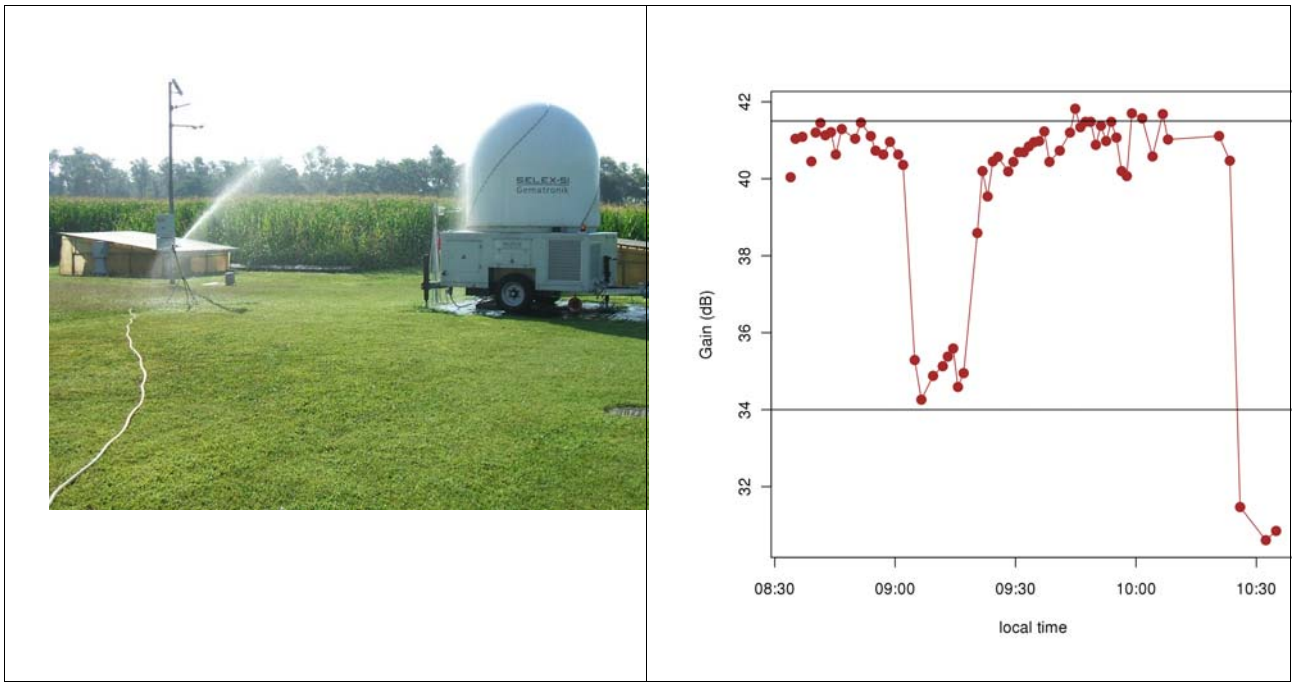

Figure 3. Left: the X-band radome irrigated with water. Right: time series of the gain during the metal sphere calibration. The drop in the power gain corresponds to the wet radome period.

The great majority of operational weather radars have their antenna unit covered by a radome. The effect of water on the radome surface has been extensively studied in the past, mainly due to the relevance of the induced attenuation for communication systems at high frequencies (Anderson, 1975, Effenberger et al., 1986; Chang, 1986). Only few studies focused specifically on weather radars (Merceret and Ward, 2000; Kurri and Huuskonen, 2008; Trabal et al., 2008). It is known that the attenuation due to the wet radome scales with operating frequency. So, while at S-band the two-way loss is in general negligible, it becomes relevant at C-band and very important at X-band. X-band radars, in addition, operate at closer ranges (typically ~50 km) than C- and S-band systems, therefore the chance to have rain on the radome is comparably higher when there is a precipitation system within the radar domain. For these reasons we attempted to estimate the induced wet radome attenuation for an X-band radar in a normal operational setup. Two distinct procedures were followed. In the first a large data set was considered and the radar reflectivity at close ranges is compared with the reflectivity calculated from the DSD measured by a nearby laser disdrometer. In the second procedure, a metal sphere was used for the radar calibration and the procedure was repeated while irrigating the radome with a sprinkler. Both procedures gave results in good

agreement with previous theoretical and laboratory studies.

The radome, although originally declared hydrophobic by the manufacturer, clearly lost its hydrophobicity properties with time. This degradation may actually occur over a relatively short period of operation, e.g. several months (Anderson, 1975). In a perspective of a dense X-band radar network, a periodical polishing of the radome surface does not appear practical. So, only two options appear viable:

- **operate the radar without the radome** (easier at X-band, due to the reduced dimensions, but still impractical in general for the higher wear and also for the "psychological" impact of a scanning antenna);
- **adopt a procedure to correct for attenuation effects in real time**. The results of this work provide some clue for the implementation of such correction.

The effects of non uniform radome wetting with azimuth and elevation (Bechini et al., 2006), e.g. due to wind direction, will also have to be considered for the implementation of a real-time correction procedure.

References

Anderson, I., 1975: Measurements of 20-GHz transmission through a radome in rain. *IEEE Transactions on Antennas and Propagation*, *vol. 23, no. 5, 619-622*.

Bechini, R., R. Cremonini, E. Gorgucci and L. Baldini, 2006: Dual-pol radar calibration and correction of the bias introduced by non uniform radome wetting. *Proceedings, 4th European Conference on Radar in Meteorology*, Barcelona, Spain, ERAD, 593-596.

Bechini R, Baldini L, Cremonini R, Gorgucci E, "Differential reflectivity calibration for operational radars," *Journal of Atmospheric and Oceanic Technology, vol. 25, pp. 1542–1555, 2008.*

Chang, K.-C., 1986. System performance in rain in a radome-enclosed environment. *International Journal of Infrared and Millimeter Waves*, v. 7, 267-289.

Effenberger, J. A., R. R. Strickland and E. B. Joy, 1986: The effects of rain on a radome's performance. *Microwave Journal*, *261-274*.

Gibble, D., 1964. Effect of Rain on Transmission Performance of a Satellite Communication System, *IEEE International Convention*. Record, Part VI, p.52.

Kurri, M. and Huuskonen, A., 2008. Measurements of the Transmission Loss of a Radome at Different Rain Intensities. *Journal of Atmospheric and Oceanic Technology* , v. 25, 1590-1599.

Merceret, F. J.; Ward, J. G., 2000: Attenuation of Weather Radar Signals Due to Wetting of the Radome by Rainwater or Incomplete Filling of the Beam Volume. *NASA/TM-2002-211171*, NASA/YA-D, Kennedy Space Center, FL, 32899, 16 pp.

Trabal, J.M., I. Zawadzki and D.J. McLaughlin, 2008: A Method to Correct for Wet Radome Attenuation in CASA Radars by the Use of a Contiguous WSR-88D Radar, ERAD 2008, Helsinki, Finland.

Waterman P.C., 1979. Matrix methods in potential theory and electromagnetic scattering. *J. Appl. Phys., v.50, p.4550-4565*.

Annex 2 - The French Project RHYTMME Experience

Introduction

The French Southern Alps is a region characterised by heavy rain and flash flood events. However, in such complex terrain the weather radar measurement error is increased significantly because of partial beam blockage, measurements made in the bright band or in snow, etc. Météo France, together with several other partners, is involved in a project called RHYTMME(Risques Hydro-météorologiques en Territoires de Montagnes et Méditerranéens) to establish a platform service for a better management of hydrometeorological hazards in this region. The RHYTMME Project aims to deploy a dense network deployment of 4 polarimetric X-band radars over the period 2010 – 2013 (see fig. 1).

The project also provides high-quality networked products (including QPE mosaics), that are integrated into automatic hydrometeorological warning systems. At present, two X-band radars are installed (in Mont Vial and Mont Maurel) and the radar production platform is running since June 2011. The raw data is concentrated in real-time in Toulouse and available for either real-time or off-line processing.

Fig.1 Map of polarimetric X-band radars network in the RHYTMME Project in 2013.

This section presents the current status of the processing chain and discusses the preliminary

results of the evaluation of various QPE algorithms. It is structured as follows: section 1 provides an overview of the current RHYTMME radar data Processing chain, section 2 discusses the adaptation of a polarimetric processing chain to X-band, section 3 describes the QPE processing chain used in the evaluation, section 4 summarizes the different QPE algorithms tested and section 5 analyses the preliminary results obtained. Finally, conclusions are discussed in section 6.

1. THE RHYTMME RADAR DATA PROCESSING CHAIN

Fig. 2 shows the flow diagram of the RHYTMME radar data processing chain.

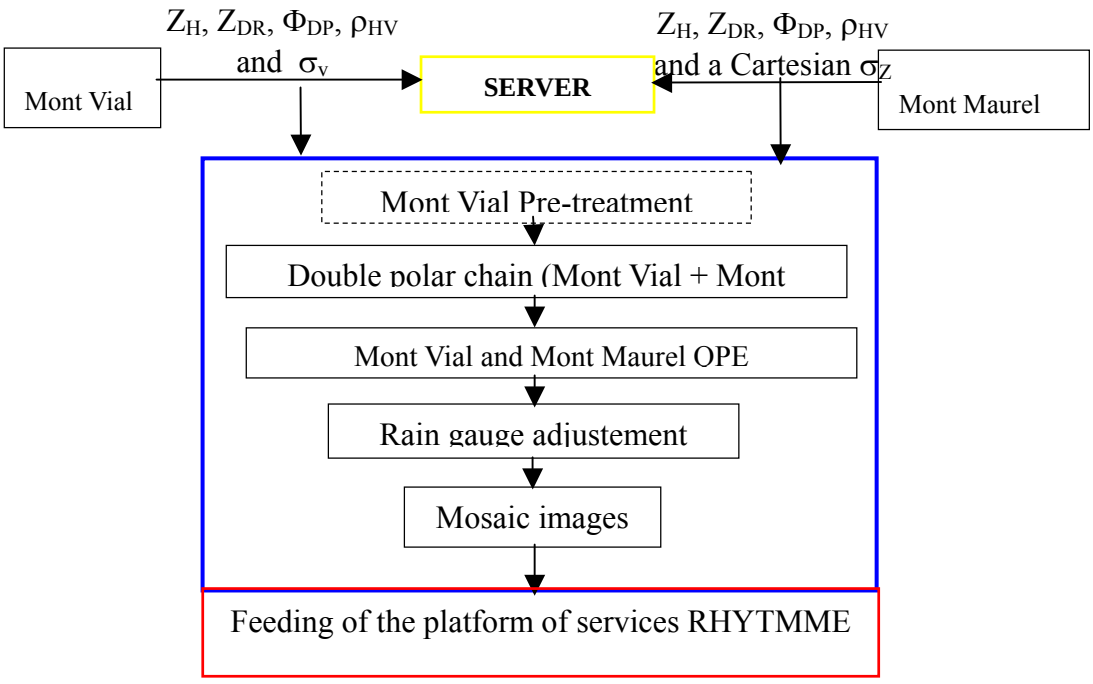

Fig. 2 The flow diagram of the RHYTMME radar data processing chain.

The polarimetric variables collected by the radars are horizontal reflectivity (Z_H), differential reflectivity (Z_{DR}), co-polar correlation coefficient (ρ_{HV}), and differential phase shift (Φ_{DP}) in polar coordinates. The radial range resolution is 300 m for Mont Vial and 240 m for Mont Maurel, while the azimuthal resolution is 0.5° for both radars. Mont Maurel also provides the standard deviation of

the reflectivity from pulse to pulse (σ_Z) at 1 km^2 resolution. In addition, Mont Vial radar provide mean Doppler velocity (v_D) and Doppler spectral width (σ_v). All this data is stored in a server and is available for off-line processing.

Since the radars in the network are heterogeneous, the first step in the processing is, if necessary, a pre-treatment of the data to make it in a uniform format so that it can be ingested into a polarimetric processing chain. The second step is the processing of the raw X-band polarimetric variables, which has been adapted from an in-house developed S- and C-band radar processing chain. The next step is to combine the processed polarimetric information available on PPIs to generate the best surface estimation of the 1 km², 5' rainfall accumulation using several polarimetric rain rate estimation algorithms.

2. THE POLARIMETRIC PROCESSING CHAIN

The modules of this processing chain are described in detail by Boumahmoud et al. (2010). Fig. 4 shows the flow diagram of the chain.

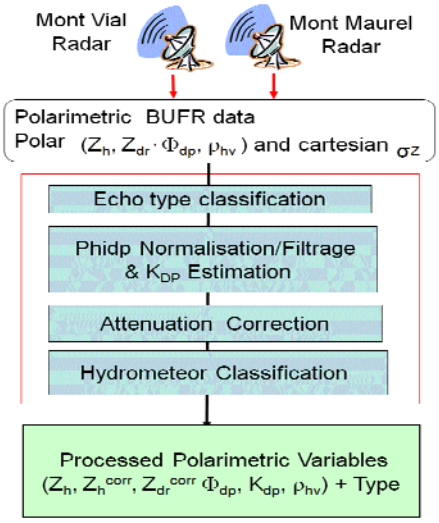

Fig. 4 Flow diagram of the Dual polar chain

The inputs of the dual-polarization chain are the polarimetric fields of Z_H, Z_{DR}, Φ_{DP}, ρ_{HV} in polar coordinates and a Cartesian field of σ_Z. It performs successively the following operations: calibration of Z_H and Z_{DR}, partial beam blockage correction using static propagation maps, non

meteorological echo identification, ρ_{HV}-based bright band identification, Φ_{DP} offset removal and filtering, K_{DP} estimation, attenuation correction, hydrometeor classification and the computation of daily monitoring indicators (Bias curves for Z_H and Z_{DR}, offset curves for Φ_{DP}, average ρ_{HV} in rain, etc.)

Since the echo type classification and the attenuation correction are strongly dependent upon the radar frequency, these modules have been adapted to the X-band.

The echo type classification is performed in two steps: a pre-classification in ground clutter, clear air and precipitation and the classification of different types of precipitation.

Gourley et al. (2007) developed the pre-classification algorithms at C-band implemented in the polarimetric chain. The scheme is based on a fuzzy logic algorithm with the particularity that the membership functions are obtained by empirical observations and objectively weighted according to the level of trust of each dataset for a particular radar site. It was observed that three parameters were the best discriminators between the different categories, ρ_{HV}, the texture of Z_{DR} and σ_Z.

The first step in the adaptation of the algorithm to X-band has been therefore to empirically obtain the membership functions for these 3 parameters. Since Mont Vial does not provide the Cartesian field of σ_Z, we decided to test other discriminating parameters and the texture of Φ_{DP} and the texture of Z_H gave satisfactory results. The correct identification of ground clutter is very important in polarimetric radars. Misidentified clutter echoes can lead to aberrant values of the precipitation field for an entire ray due to the resultant wrong attenuation correction. On the other hand, the identification of precipitation as clutter leads to gaps in the rain field, which is a serious issue in areas that already suffer heavily from clutter.

The hydrometeor classification is also performed using fuzzy logic. If the use of fuzzy logic precipitation classification at S and C band can be considered relatively mature the same cannot be said at X band due to the relatively recent interest of the community for such frequency band. Météo France is currently developing and evaluating the performance of an new algorithm (Al-sakka et al. 2011). In this study, the used hydrometeor classification is an algorithm developed by Snyder et al. (2010) which could be considered an extension of the algorithm by Park et al. (2009) to X-band.

The attenuation correction, at this stage, is performed using a simple static empirical linear

relationship between the path-integrated attenuation (and differential attenuation) and Φ_{DP}. Both the specific attenuation and the specific differential attenuation are considered proportional to Φ_{DP} with a constant of proportionality (γ_H for the specific attenuation and γ_{DP} for the specific differential attenuation respectively) that is frequency dependent (Ryzhkov & Zrnic 1995). The value of γ_H was experimentally estimated using the Mont Vial radar data from scatter plots of measured Z_H versus Φ_{DP} to be 0.28. The value of γ_{DP} was deduced from ratios of γ_H/γ_{DP} appeared in literature (Bringi & Chandrasekar, 2001) and Snyder et al. (2010). We chose $\gamma_{DP} = 0.04$.

The polarimetric chain outputs are Z_{DR} and Z_H (with and without attenuation correction), ρ_{HV}, offset corrected and filtered (using a running median filter of about 6 km) Φ_{DP}, estimated K_{DP}, texture of Z_{DR}, the estimated path-integrated attenuation and differential attenuation, σ_Z and the echo type classification in polar coordinates. The corrected Z_H, the echo type and the Path Integrated Attenuation (PIA) are also provided, in Cartesian coordinates.

3. The QPE Processing Chain

A polarimetric QPE processing chain, designed for evaluation purposes, that obtains hourly precipitation accumulation estimation from single tilts has been implemented (Figueras et al., 2011). Its flow diagram is shown in Fig. 5.

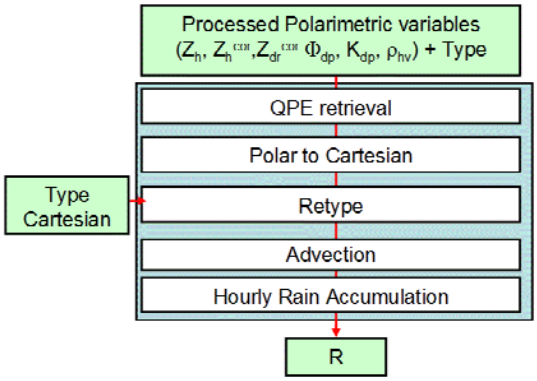

Fig.5 Flow diagram of the QPE processing

The inputs of the algorithm evaluation are the outputs of the polarimetric pre-processing chain. The first step is to estimate the instantaneous rainfall rate in areas classified as precipitation using one of the implemented algorithms (see section 5). The outputs of the algorithm are then

transformed from polar to Cartesian coordinates using the Cressman Analysis. At this point, the data is re-evaluated according to the echo type. Pixels classified as noise, single polarization (low SNR), sea clutter and clear air are re-assigned from missing value to 0 mm/h rainfall rate. To compensate for the advection between measurements, a temporal interpolation is performed using an advection field calculated a priori from the evolution of the previous reflectivity measurements. The interpolated rainfall rate field is added and thus the 5 minute precipitation accumulation is obtained. It follows the addition of the twelve 5 minutes precipitation accumulation fields to obtained the hourly rainfall accumulation. The hourly rainfall accumulation can then be compared with the hourly rainfall accumulation obtained by the high density network of rain gauges operated by Météo France.

This comparison is done on a collocated pixel basis and the maximum distance from the radar system evaluated is 60 km. Only one elevation angle is used in the evaluation. The quality of the algorithms is evaluated based on the normalized bias between the rain gauge and the radar retrieved rainfall accumulation (NB) defined as:

$$NB = \frac{\langle R \rangle}{\langle G \rangle} - 1$$

and the correlation (corr):

$$corr = \frac{\sum_{\forall i} \left(G_i - \langle G \rangle\right)\left(R_i - \langle R \rangle\right)}{\sqrt{\sum_{\forall i} \left(G_i - \langle G \rangle\right)^2} \sqrt{\sum_{\forall i} \left(R_i - \langle R \rangle\right)^2}}$$

4. Tested Polarimetric QPE Algorithms

At this stage, 2 families of algorithms have been implemented: 1) simple Z-R relations with and without attenuation correction based on Φ_{DP}, 2) algorithms based on the relation between rainfall rate (R) and K_{DP}. In addition, a synthetic algorithm has been implemented combining R-K_{DP} and Z-R relations with attenuation correction. It is based on a threshold on K_{DP} (0.5º/km, approximately 10 mm/h). Below the threshold level, Z-R relations are used and above it R-K_{DP} relations are used instead.

To summarize, we have tested 8 algorithms:

- Two different Z-R relations with and without attenuation correction (Marshall-Palmer and the relation used by the American WSR-88D radars, i.e. 200 $R^{1.6}$ and 300$R^{1.4}$)

- Two R-K_{DP} relations of the form $R=a(K_{DP}/f)^b$ (From Bringi and Chandrasekar 2001): One for the Beard-Chuang equilibrium shape model (a=129, b=0.85) (Beard and Chuang, 1987) and another corresponding to the Brandes equilibrium shape model (a=132, b=0.791) Brandes et al. (2002), with f=9.375 GHz.

- Four synthetic algorithms Z-K_{DP} :
  - Z-K_{DP}1 : Marshall-Palmer (Att. corr.MP) and Beard et Chuang.
  - Z-K_{DP}2 : Marshall-Palmer (Att. corr. MP) and Brandes et al.
  - Z-K_{DP}3 : Fulton et al. (Att. corr WSR-88D) and Beard et Chuang.
  - Z-K_{DP}4 : Fulton et al. (Att. corr. WSR-88D) and Brandes et al.

5. **Preliminary results**

Presented here are preliminary results obtained from selection of 4 events (10 days) of precipitations (mostly intensive precipitation) occurred in the vicinity of Mont Vial Radar.

All the results are stratified according to 4 ranges on the rain gauge hourly accumulations: [0.2, 1[, [1, 5[, [5, 10[and >10 mm/h. Notice that for small intervals the correlation does not provide meaningful results.

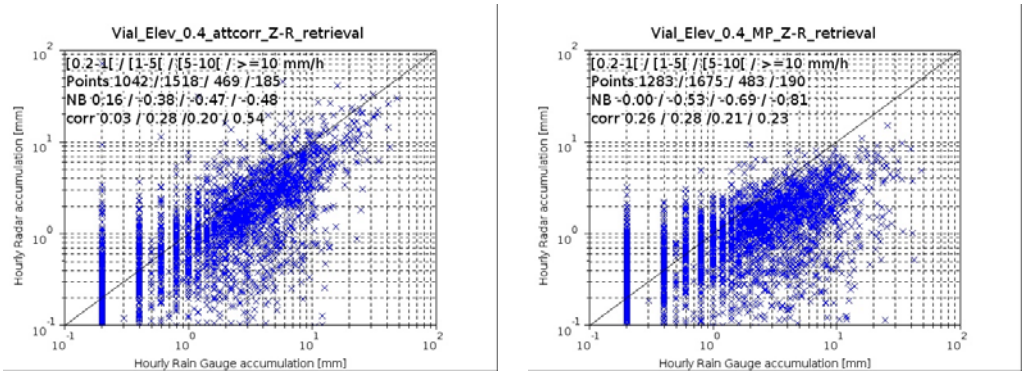

Fig.6 QPE results : (a) MP,(b) Att. corr. MP

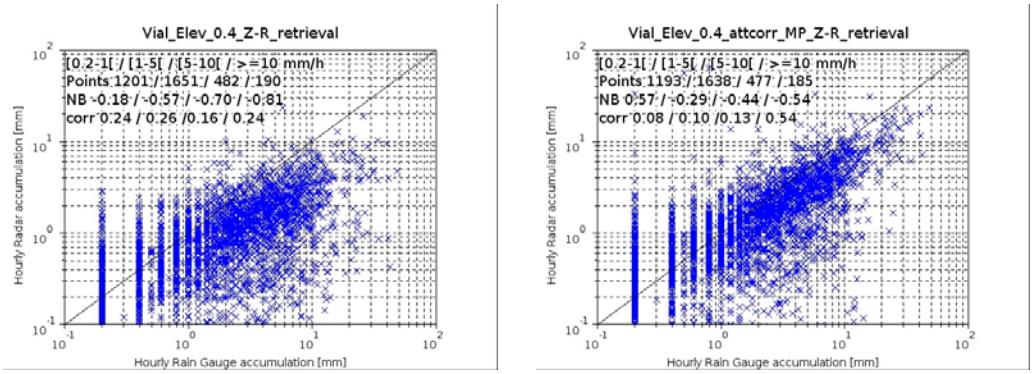

Fig.7 QPE results : (a) WSR-88D, (b) Att. corr. WSR-88D

Figures 6 and 7 summarizes the results obtained by Marshall-Palmer and the relation used by the American WSR-88D radars (without attenuation correction and with attenuation correction and partial beam blockage correction). It can be observed that:

- Without attenuation correction, Marshall-Palmer scores are equivalent to the WSR-88D scores.

- The attenuation correction significantly improves the correlation between rain gauge and radar retrieved measurements, particularly at higher precipitation rates. There is also an improvement of the bias.

- The benefit of the partial beam blockage correction is self evident, since there is a remarkable improvement of both the correlation and the bias.

Figure 8 summarizes the results obtained by R-K_{DP} relation (Beard and Chuang) and synthetic algorithms Z-K_{DP}1 and Z-K_{DP}3 while Figure 9 summarizes the results obtained by R- K_{DP} relation (Brandes et al.) and synthetic algorithms Z-K_{DP}2 and Z-K_{DP}4.

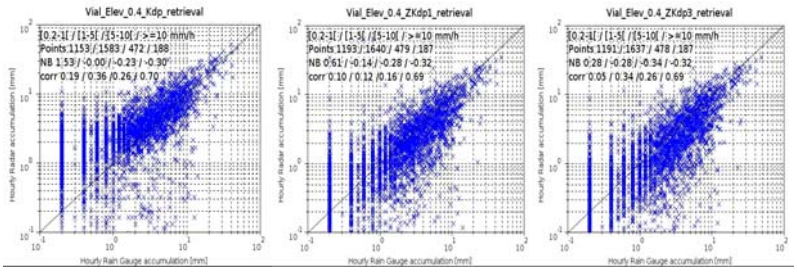

Fig. 8 QPE results : (a) Beard and Chuang relation , (b) synthetic algorithm Z-K_{DP}1 and (c) Z-K_{DP}3

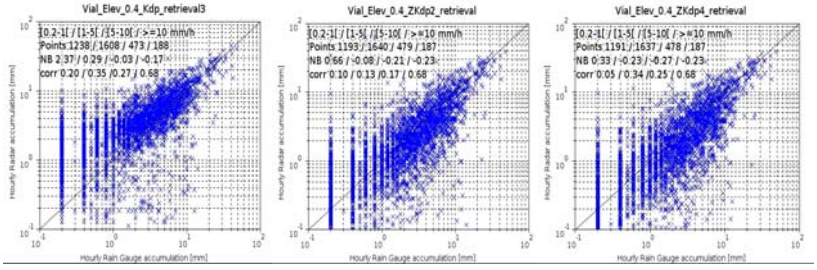

Fig. 9 QPE results : (a) Brandes et al. relation , (b) synthetic algorithm Z-K_{DP}2 and (c) Z-K_{DP}4

These results show that:

- In general terms the R-K_{DP} algorithms show an improved correlation with respect to the other tested algorithms, particularly at higher precipitation rates (above 10 mm/h).

- The evaluation of the results of a synthetic Z-K_{DP} algorithm shows that the combination of Attenuation corrected Marshall-Palmer and Brandes et al. are the best both in terms of correlation and bias.

6. Conclusion

This section has presented the current status of development of a polarimetric radar network data processing chain to provide accurate QPE to decision makers in a flooding-prone mountainous region. We as well summarize the results of several Pol-QPE algorithms that have been preliminary tested, which are based on simple Z-R relationships and on K_{DP}.

K_{DP} has shown to be a very good candidate because it is insensitive to calibration errors and partial beam blocking. A synthetic Z-K_{DP} algorithm, which combines R-K_{DP} relations for intense precipitation and Z-R relations corrected for attenuation in the weak rain, has been tested and the one which shows the best score is Z-K_{DP}2 (combination of Attenuation corrected Marshall-Palmer and Brandes et al.).

The next step will be to enhance the evaluation including more events and testing other polarimetric precipitation estimation algorithms, such as the integrated ZZDR technique by Illingworth & Thompson (2005), the variational approach (Hogan, 2007) and ZPHI (Testud et al. 2000).

Once the optimal algorithm is determined, the implementation of intelligent compositing rules

between X-band radars, allowing for a mitigation of attenuation effects and optimal exploitation of the network will be studied. Maps of minimum detectable signal will also be produced and used in the compositing rules in order to mitigate situations of severe attenuation/extinction leading to complete misses of precipitation detection by one particular radar.

Finally, the fact that, among the two already installed radars, one has a radome and the other one does not opens perspectives in the quantitative evaluation of wet radome attenuation on polarimetric measurements.

References

Alsakka H., F. Kabeche, J. Figueras i Ventura, B. Fradon, A. A. Boumahmoud, and P. Tabary., 2011: A simple-but-realistic fuzzy logic hydrometeor classification scheme for the French X, C and S-band polarimetric radar. In Proceedings of 35nd Conference on Radar Meteorology, Pittsburgh, PA, 26-30 Sept. 2011 *American Meteorological Society: Boston.* MA.

Beard KV, Chuang C., 1987: A New Model for the Equilibrium Shape of Raindrops. *J. Atmos. Sci*. 44: 1509-1524.

Boumahmoud A.-A., Fradon B., Roquain P., Perier, L., Tabary P., 2010: French operational dual-polarization chain. European Conference on Radar in Meteorology and Hydrology. *ERAD2010*.

Brandes EA, Ryzhkov AV, Zrnic DS., 2001: An Evaluation of Radar Rainfall Estimates from Specific Differential Phase. *J. Atmos. Oceanic Technol*., 18: 363-375.

Bringi V.N., Chandrasekar V., 2001: Polarimetric Doppler Weather Radar: Principles and Applications. *Cambridge University Press.*

Figueras i Ventura J, Boumahmoud A-A, Fradon B, Tabary P., 2011: Long-term monitoring of French polarimetric radar data quality and evaluation of several polarimetric quantitative precipitation estimators in ideal conditions for operational implementation at C-band. Submitted to Quarterly. *Journal of the Royal Meteorological Society*.

Gourley JJ., Tabary P., Parent-du-Chatelet J., 2007: A fuzzy logic algorithm for the separation of precipitating from non-precipitating echoes using polarimetric radar, J. Atmos. Oceanic Technol. Vol. 24, No.8, 1439–1451.

Hogan, R.J., 2007: A Variational Scheme for Retrieving Rainfall Rate and Hail Reflectivity Fraction from Polarization Radar. J. Appl. Meteor., Vol. 46, 1544-1563.

Illingworth A.J., Thompson R.J., 2005: The Estimation of Moderate Rain Rates with Operational Polarisation Radar. Proceedings of the 32th Conference on Radar Meteorology.

Ryzhkov, A. V., and D. S. Zrnic., 1995: Precipitation and attenuation measurements at 10-cm wavelength. *J. Appl. Met.*, Vol. 34, 2121–2134.

Snyder, J. C., H. B. Bluestein, G. Zhang, and S. J. Frasier., 2010: Attenuation correction and hydrometeor classification of high-resolution, X-band, dual-polarized mobile radar measurements in severe convective storms. *J. Atmos. Oceanic Technol*., 27, 1979–2001.

Testud, J., Le Bouar E., Obligis E., and Ali-Mehenni M., 2000: The rain profiling algorithm applied to polarimetric weather radar, *J. Atmos. Oceanic Technol*., Vol. 17, 332-356.

Annex 3 - The effect of a wet radome on dualpol data quality

1. Introduction

Operational radar systems typically are equipped with a radome. A radome protects the radar system and allows continuous operation under all weather conditions. The potential disadvantage of using a radome is that it may affect the outgoing and incoming microwave, in particular when the radome is wet. Radomes are typically optimized to minimize the transmission loss and to avoid azimuthal variations of the received signal due to radome seams. Furthermore, the radome material is chosen to be hydrophobic, in order to avoid as much as possible additional attenuation due to a wet radome surface. Radome attenuation is discussed in a number of papers where the effect typically is analyzed under idealized conditions (e.g. Manz, 2001). The level of attenuation will also depend on rainfall intensity and type. The dependence on rainfall intensity has been investigated recently in Kurri and Huuskonen (2008). Under operational conditions, the attenuation of the radar signal may depend on elevation and azimuth. For example, attenuation may be quite heterogeneous under strong wind conditions because the radome is not equally wet (e.g. Germann (2000). The effect wet radome attenuation on polarimetric moments so far has not been investigated in detail.

In this work we investigate the effect of radome attenuation on polarimetric moments under operational conditions. Data are taken from the dualpol C-band radar at the Hohenpeissenberg Meteorological Observatory . This radar is the research radar of the German Met. Service, DWD. The radar is protected by a 12-year old radome of orange-peel type. No dedicated maintenance has been applied to this radome. Eleven months of radar data are analyzed and statistics are computed to identify the mean attenuation of a wet radome and its variability. Variability may be expected due to the meteorological conditions at the radar site (e.g. wind) or due to the type of hydrometeors (e.g. snow vs. rain).

2. The data

Data from February to December 2008 are analyzed. We perform 5 minute volume scans in STAR (Simultaneous Transmitt and Receive) mode. In STAR mode, each volume contains 10 elevation angles. The main characteristics of the scan definition are briefly described here:

STAR-Mode (every 5 min), with the following settings:

- 10 elevation angles: 0.5◦, 1.5◦, 2.5◦, 3.5◦, 4.5◦, 5.5◦, 8◦, 12◦, 17◦, 25◦
- elevation angles 0.5 - 4.5◦: PRF = 640 Hz, AZ-rate 16◦/s, range= 230 km.
- elevation angles 5.5 - 25◦: PRF = 1160 Hz, AZ-rate 16◦/s, range= 128 km.
- Raw-range bin resolution: 125 m
- Range averaging: 250 m.
- pulse width: 0.8 μs
- Dynamic angle synching (DAS) with 1◦ ray width. 1

The following moments are available:

- CZH,CZV,UZH,UZV, VH, V V,WH,WV,
- DP ,ZDR, □HV ,KDP , with
- CZH,CZV : clutter corrected reflectivity factor Z, horizontal (H) and vertical V) polarization.
- UZH,UZV : un-corrected reflectivity factor Z, horizontal (H) and vertical V) polarization.
- V H, V V : line-of-sight Doppler velocity, from horizontal (H) and vertical V) polarization.
- WH,WV : Doppler spectral width, from horizontal (H) and vertical V) polarization.
- ZDR: Differential reflectivity.
- Phi_{DP} : Differential phase.
- KDP : Specific differential phase.
- RHO_{hv}: Cross-correlation coefficient.

The reference precipitation measurement is a rain gauge at the radar site. These data with one-minute resolution are used to define the onset and end of a precipitation event over the site. Furthermore, the independent precipitation data allow the classification of the attenuation effect with respect to precipitation rate.

3. Case study with moderate precipitation

Two screenshots of ZDR taken 25.4.2008 just before and during precipitation at the radar site are shown in Figure 1. The situation was characterized by strong graupel showers. From literature (e.g. Bringi and Chandrasekar, 2001) it is known that graupel is typically characterized by slightly negative or near zero ZDR which is consistent with the ZDR-values before the precipitation reaches

the radar site. During the precipitation event at the site, ZDR becomes positive which can be attributed to differential radome attenuation of ZH and ZV because the character of precipitation (graupel) did not change.

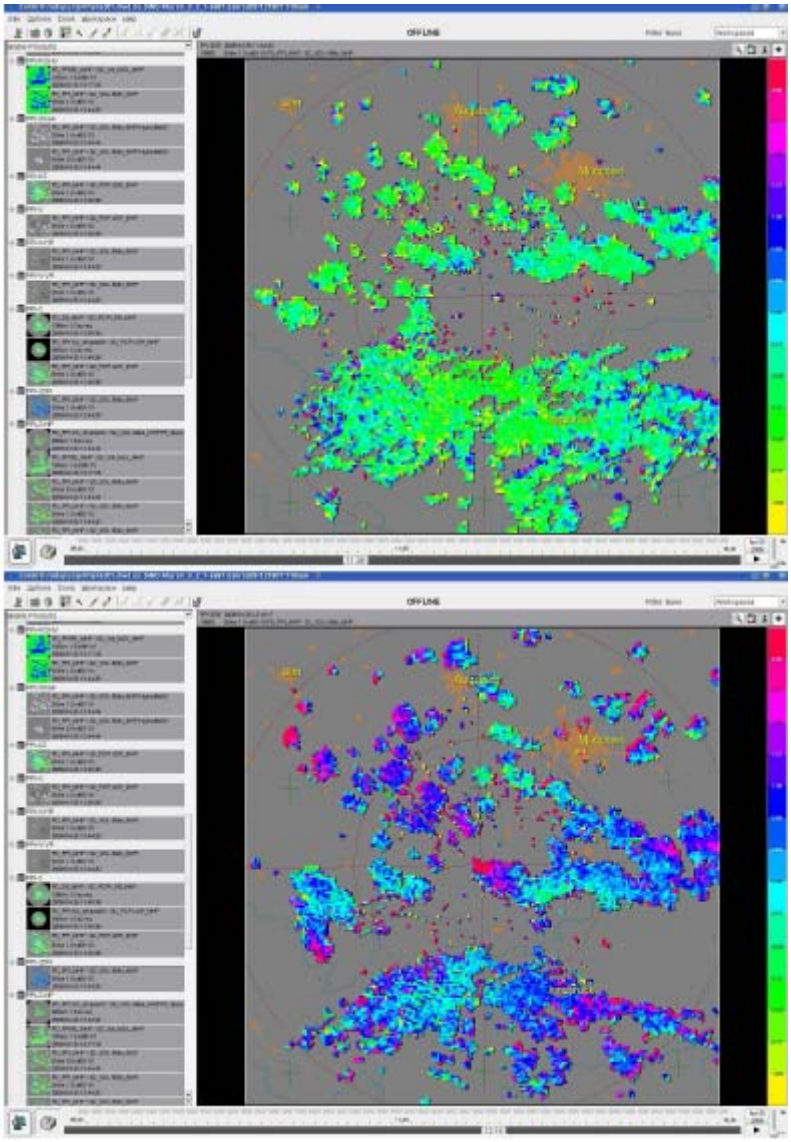

Figure 1: ZDR [dB] screenshots taken 25.4.2008 before the precipitation event reaches the site (left) and while the event is over the site (right). The scale of ZDR is from -1 (yellow) to +2 (red).

A more quantitative impression on the magnitude of attenuation is shown in Figure 2. Here we compute sweep averages of radar moments at el = 1.5◦. In order to reduce scatter due to bad signal quality and clutter we only consider data at r > 4 km, □HV > 0.8 and z < 12000 m.

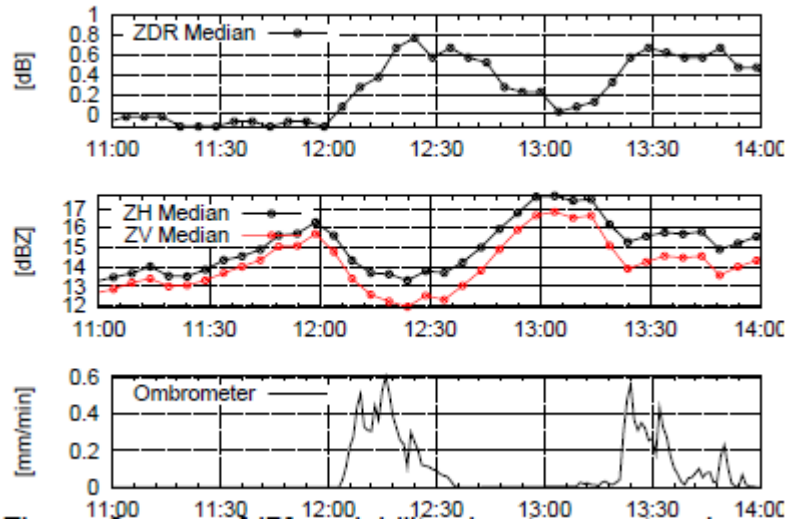

Figure 2: ZDR [dB] variability due to a wet radome. Before the precipitation reaches the radar site, ZDR is slightly negative. During the precipitation event ZDR becomes positive (ZDR 0.8).

We make the assumption that there is no overall change in precipitation type and intensity as seen by the radar. As such, any variations are attributed to the radome effect. As a reference we show the rain-gauge measurements at the radar site. Once the precipitation reaches the site, we notice a decrease of ZH and ZV of about 3 and 4 dB, respectively. ZV attenuation is stronger which is highlighted by the increase of ZDR up to a value of 0.8 dB. Stronger ZV attenuation can be attributed to the more or less vertically aligned water runoff from the radome. From Figure 2 we can also deduce a drying time of the radome on the order of 30 min which can be related to the time it takes to reach again the magnitudes of the radar moments as observed just before the precipitation event reaches the site. RHOHV shows a weak decrease (not shown) and there is no clear picture seen in PHIDP.

4. Case study with intense precipitation

As another example we consider an event of very intense precipitation (up to 4 mm/min) observed on 17.5.2008. We again show two screenshots of radar products before and while the cell is over the radar site (Figure 3).

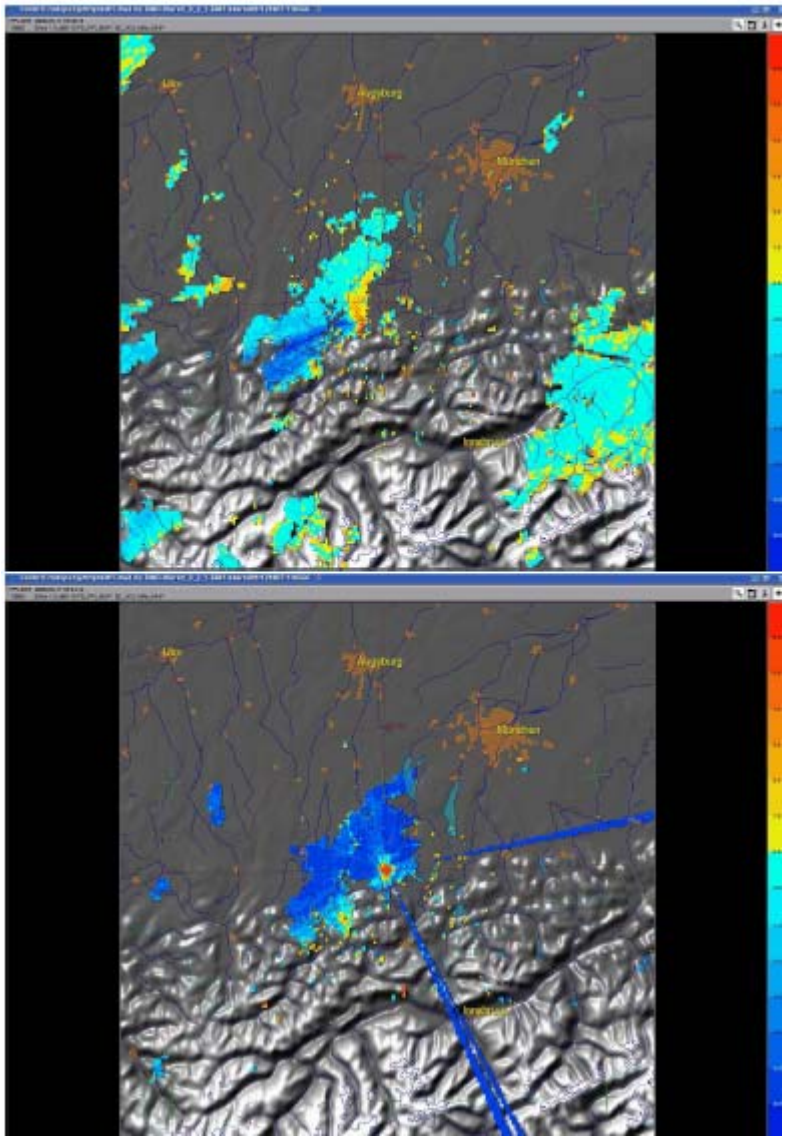

Figure 3: ZDR [dB] screenshots taken 17.5.2008 before the precipitation event reaches the site (left) and while the event is over the site (right), 17.5.2008. The scale of ZDR is from -6.4 (blue) to +6.4 (red). Zero ZDR codedwith as yellow.

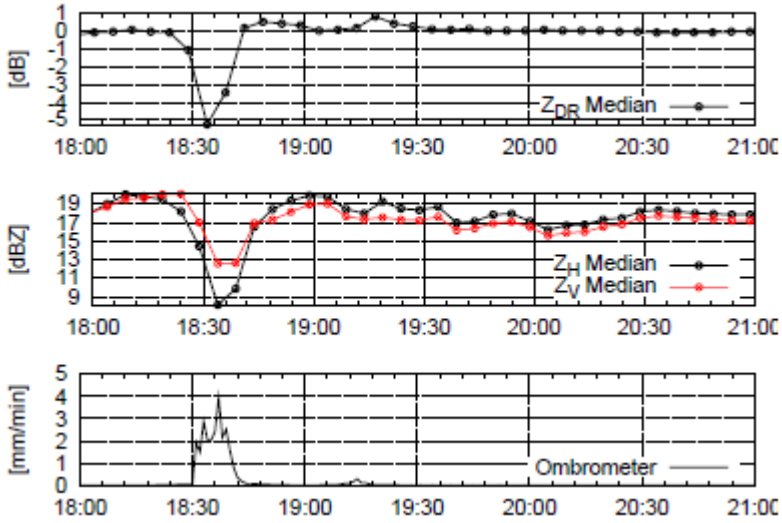

Figure 4: ZDR [dB] bias during an intense precipitation event.

Note that we use a different color scale compared to the one of Figure 1. There are a number of features readily visible from Figure 3. First of all we see strong attenuation effects in ZDR (blue colors behind the leading edge of the cell south-west from the radar site). The leading edge of the cell is characterized by large positive ZDR values (up to +5 dB), which is indicative of large drop sizes including possibly hail. This corresponds to drop sizes of $\approx 6 - 8$ mm (Bringi and Chandrasekar, 2001). When the cell is over the site, ZDR assumes large negative values (≈ -5 to -4 dB). We furthermore observe ray-shaped disturbances when the cell is over the site. Those disturbances appear to be not coherent, as they are not visible in the Doppler moments. The source of those echoes appears related to a shielding problem which has been fixed in the meanwhile. Similar to the previous case we compute sweep averaged values of each radar moment, in order to quantify the relative magnitude changes for each moment. The time series of Z,ZDR and ombrometer data (Figure 4) substantiate the more qualitative view of the screenshots (Figure 3). Here we find a strong negative bias in ZDR. The attenuation of ZH is significantly stronger than for ZV . The overall attenuation of ZH is on the order of 10 dB which is due to a combination of the wet radome effect and the path attenuation by

the cell itself. A large negative ZDR deviation is already observed before the precipitation reaches the site. The contribution of the wet radome to the ZDR bias is difficult to quantify in this

case. The data suggest that the microphysical structure of the cell and the associated attenuation dominate the (negative) ZDR bias. This is different from the previous case where we find positive ZDR. The weak/moderate precipitation event starting around 19:15 UTC shows a positive ZDR bias consistent with the previous case study.

5. Statistical analysis

a. Bias as a function of time

We analyze the effect of radome attenuation considering all precipitation events from February to December 2008. The data sample is expected to be rather heterogeneous so we initially define criteria to isolate specific precipitation events from the data. We only consider precipitation events that have at least a duration of 10 minutes. Furthermore, we require a period of 30 minutes without any precipitation at the radar site prior the precipitation event. The 30 minute sequence is defined as the dry radome reference where radar data is expected to be affected solely by the radome design characteristics. Applying these criteria to the data we obtain about 70 samples for further analysis which is still a rather small sample size for a statistical analysis. Nevertheless we perform some basic analysis in order to identify basic properties of the radome attenuation effect. For these samples, the average accumulated rain and its range is shown in Figure 5. In the following we consider only the first 30 minutes after the beginning of a precipitation event. The analysis is carried for four elevation angles: 0.5◦ (sweep 9), 1.5◦ (sweep 8), 2.5◦ (sweep 7) and 8◦ (sweep 3).

The corresponding relative change of ZDR as a function of time is shown in Figure 6 for sweep 8. This moment is impacted most by a wet radome. The ZDR bias increases initially more or less linearly for the first 20-30 minutes before maximum attenuation for a given rain event is reached. The average differential attenuation is +0.3 dB. Considering a required accuracy of 0.1 dB for ZDR, wet radome attenuation has to be considered and should be corrected for in operational applications.

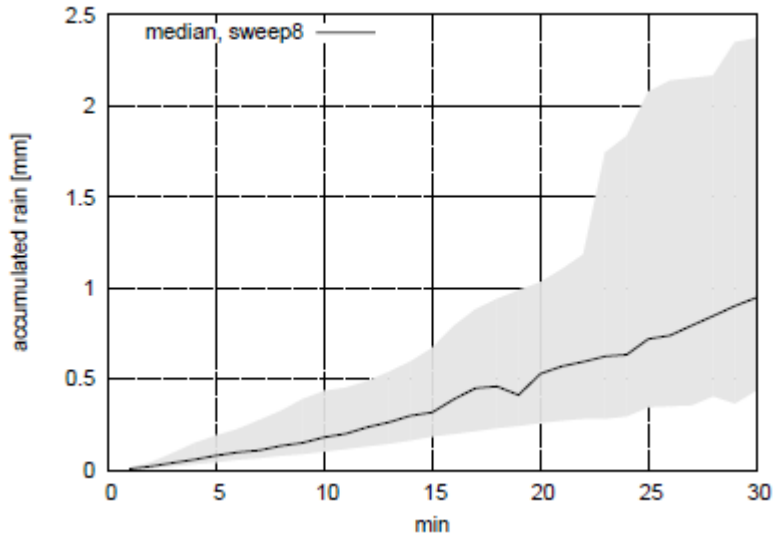

Figure 5: Average accumulated rain (median) and the distribution of rain amounts for the samples to study radom attenuation. The range is defined by the 1st and third quartile of the distribution at a given time. the radome.

The spread in ZDR bias suggests that the bias is dependent on the actual rain rate and other meteorological effects which may lead to a heterogeneous wettening of radome. The dependence on rain rate will be investigated in the next section.

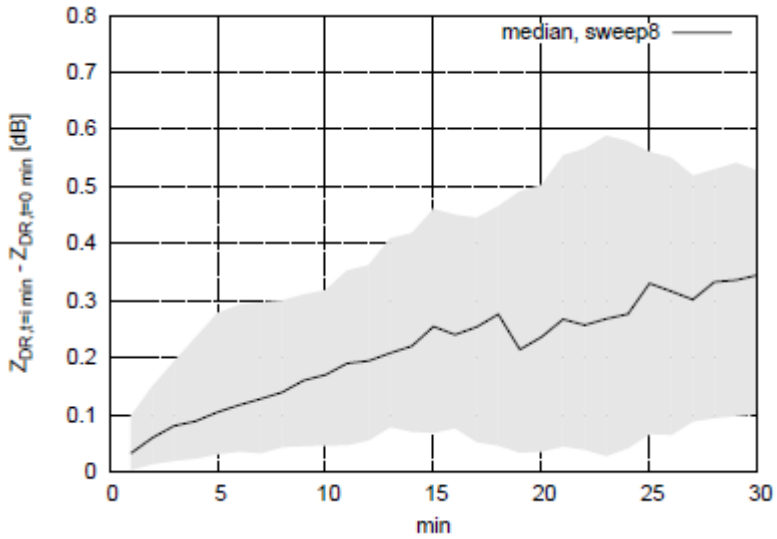

Figure 6: ZDR change relative to the average "dry" ZDR

For illustrative purposes we show also the variation of RHOHV which does not show a

comparable systematic behavior as a function event time (Figure 7).

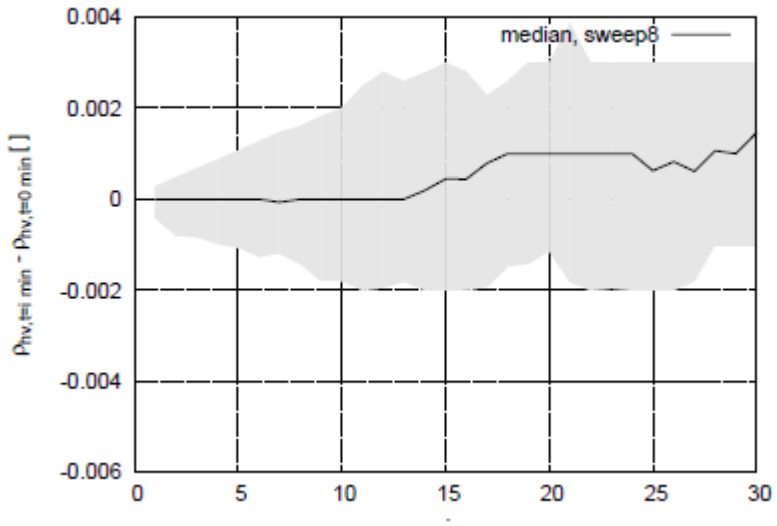

Figure 7:PHIDP and RHOHV change relative to the average "dry" values

Here deviations on the order of 0.002 are observed due to radome attenuation which is smaller than the required accuracy (0.005) but which adds to the overall uncertainty in RHOHV from other components in the radar system. b. Bias as a function of elevation angle In principle, the influence of wet radome may be elevation dependent as the water coating of the radome will be variable. This may be due to variable exposure of a radome element to the precipitation event, e.g. whether it is up or downstream of the main atmospheric flow. This is an aerodynamic effect which may cause variable radome water coating as a function of azimuth and elevation. Furthermore an elevation dependent water coating can be expected as more and more water is collected while the water drains off from the radome due to gravitation. This water runoff is collected in little streams which may cause an additional azimuthal dependence in attenuation.

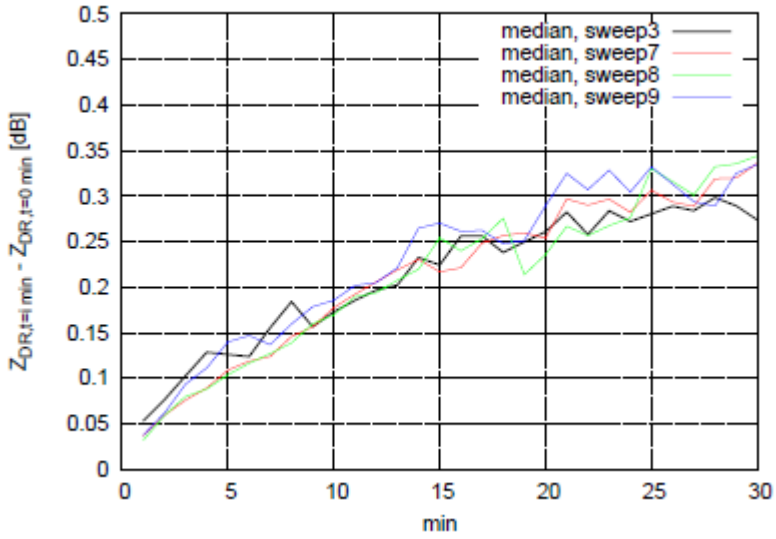

Figure 8: ZDR [dB] bias as function of four elevation angle: sweep 3 (8◦), 7 (2.5◦), 8 (1.5◦) and 9 (0.5◦).

In principle, the analysis of the elevation dependence could take into account wind speed as a further variable. This may be considered at a later stage of the analysis when a larger data set is available. The analysis of the four elevation angles shows no distinct differences for ZDR (Figure 8). This would suggest an elevation independence of ZDR attenuation at least for the sample considered here. Previous case studies show that the bias is a function of rain rate. We therefore analyze the sample with respect to rain rate focusing on ZDR. The results are shown in Figure 9.

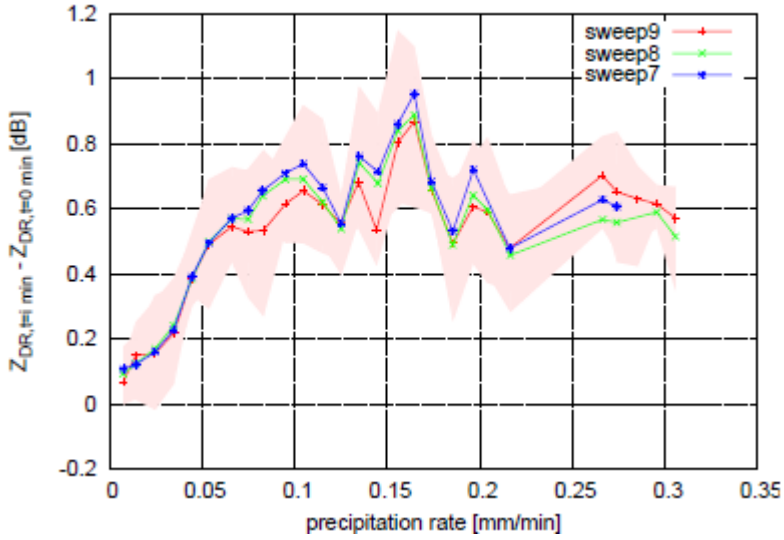

Figure 9: ZDR [dB] bias as a function of rain rate, including snow cases. Shown is the bias at lower elevation angels.

Up to a rain rate of ≈ 0.15 mm/min, there is a steady increase of ZDR bias up to a level of 0.6 dB. On average, this bias remains constant for larger rain rates (saturation effect). The scatter is relatively large for larger rain rates due to a small sample size. Since our sample also includes a number of snow cases, we carried out a sensitivity study by removing the snow samples. The result is shown in Figure 10. Snow cases are mainly related to small precipitation rates. Removing those samples leads a more or less linear bias increase as a function of rain rate (up to ≈ 0.1 mm/min). This feature may be used for a correction scheme to correct for the ZDR bias.

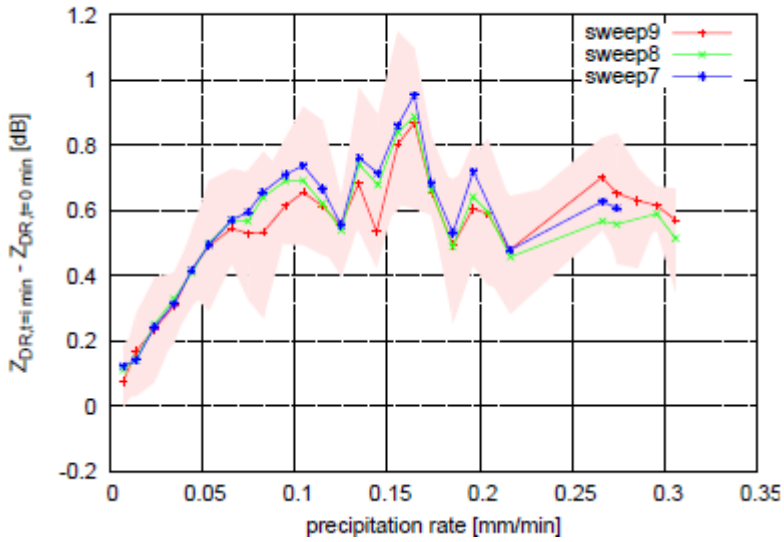

Figure 10: ZDR [dB] bias as a function of rain rate, excluding snow cases. Shown is the bias at lower elevation angles.

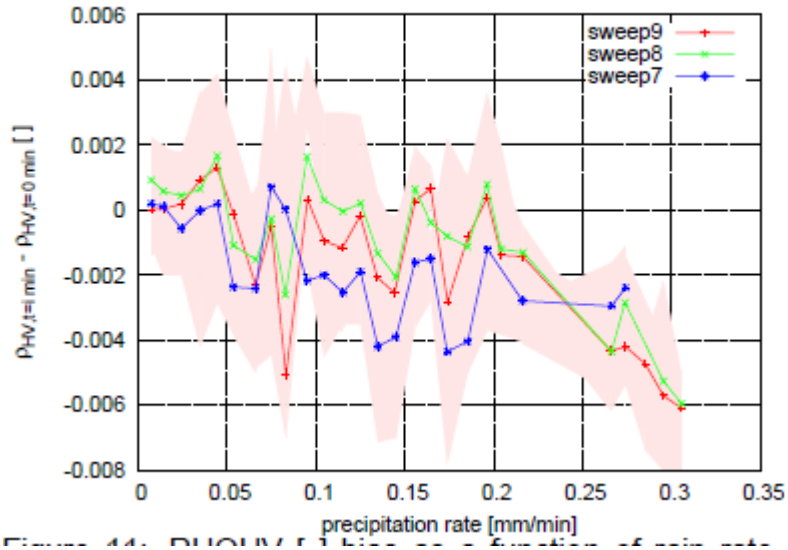

Figure 11: RHOHV [ ] bias as a function of rain rate. Shown is the bias at lower elevation angles.

We also analyze the dependence of RHOHV on rain rate. The result is shown in Figure 11. There is no clear trend visible. At large rain rates there appears to be a -0.2 bias towards smaller RHOHV values, but on average the magnitudes are small and still within the target accuracy.

6. Summary

In this paper we have analyzed the impact of a wet radome on dualpol moments. The largest impact is identified for ZDR. We have shown that there can be significant bias in ZDR as a function of rain rate. The bias can be as high as +0.8 dB or more. Algorithms (HMC, QPE) that rely on ZDR are certainly affected by such a bias. A correction of ZDR appears necessary. Other dualpol moments such as RHOHV and PHIDP appear, at least for our samples, weakly affected by a wet radome. The ZDR bias as a function of rain rate basically shows a linear increase up to a rain rate of ≈ 0.1 - 0.15 mm/min. The observed bias is due to a 12 year old orange-peel radome that has never been maintained. In that respect, the results emphasize the necessity of high quality hydrophobic surface coating and the consideration of preventive radome maintenance to minimize the impact of a radome on dualpol moments (in particular the differential moments). The presented results serve

as a reference data set against which the radomes of the new DWD weather radar systems will be evaluated.

References

Bringi, V. N. and V. Chandrasekar: 2001, Polarimetric Doppler Weather Radar . Cambridge University Press, 636 pp.

Germann, U.: 2000, Spatial continuity of precipitation, profiles of radar reflectivity and precipitation measurements in the Alps. Ph.D. thesis, Swiss Federal Institute of Technology (ETH), Z¨urich.

Kurri, M. and A. Huuskonen: 2008, Measurements of the transmission loss of a radome at different rain intensities. J. Atmos. Ocean. Tech., 25, 1590 – 1599.

Manz, A.: 2001, Radome influence on weather radar systems, principles and calibration issues. AMS Workshop Radar Calibration, Albuquerque, NM, USA, p8. 7

Annex 4 - X-band survey

ID	Country	CID	WMO code	Owner	Location	Status	Latitude	Longitude	Altitude (m)	Doppler (Y/N)	Polarization (Y/N)
1	Belgium	LAWR		Aquafin NV	Leuven	3	50°52'40"	4°42'55"		N	N
2	Denmark	LAWR		DHI	Virring	1	56,024 N	10,0246 E	142	Y	N
3	Denmark	LAWR		Municipality of Egedal	Egedal	1				Y	N
4	Denmark	LAWR		Municipality of Hørsholm	Hørsholm	1				Y	N
5	Denmark	LAWR		Municipality of Hvidovre	Hvidovre	1				Y	N
6	Denmark	LAWR		Municipality of Odense	Odense	1				Y	N
7	Denmark	LAWR		Municipality of Arhus	Arhus	1				Y	N
8	Denmark	LAWR		Municipality of Vejle	Vejle	1				Y	N
9	France	Rainscanner		Eurocorps	Mobile	1	mobile	mobile	mobile	N	N
10	France	METEOR 50DX		Meteo France	Alpine area					Y	Y
11	France	METEOR 50DX		Meteo France	Alpine area					Y	Y
12	France	METEOR 50DX		Meteo France	Montagne Maurel	1	44,02 N	06,54 E	1773	Y	Y
13	France	Rainscanner		Meteo France	Mobile	1	mobile	mobile	mobile	N	N
14	France	Hydrix		CNRS	Mt. Vial	1	43,8951	7,1529	1500	Y	Y
15	Germany	METEOR 50DX		DWD	Frankfurt	1				Y	Y
16	Germany	METEOR 50DX		DWD	Munich	1				Y	Y
17	Germany	Rainscanner		FZ Garmisch	Garmisch-Partenkirchen	3	47,73 N	11,03 E	923	N	N
18	Germany	Rainscanner		FZ Jülich	Jülich	3	50,50 N	6,33 E	619	N	N
19	Germany	Rainscanner		FZ Leipzig	Leipzig	3				N	N
20	Germany	Rainscanner		Institut für Wetter und Klimakommunikation	Hamburg	1	53,57 N	9,99 E	21	N	N
21	Greece	XPOL		NOA - IERSD	Athens	1	mobile	mobile	mobile	Y	Y
22	Italy	METEOR 50DX		Arpa Piemonte	Mobile	1	mobile	mobile	mobile	Y	Y
23	Italy	ELDES- WR-10X		ARPAV	Valeggio s.m. (VR)	1				N	N
24	Italy	METEOR 50DX		DPC	Mobile	1	mobile	mobile	mobile	Y	Y
25	Italy	METEOR 50DX		DPC	Mobile	1	mobile	mobile	mobile	Y	Y
26	Italy	METEOR 50DX		DPC	Mobile	1	mobile	mobile	mobile	Y	Y
27	Italy	METEOR 50DX		DPC	Mobile	1	mobile	mobile	mobile	Y	Y
28	Italy	ELDES- WR-10X		DPC FVG	Mt. Lussari UD	1				N	N
29	Italy	ELDES- WR-10X		Epson Meteo	Milano	1				N	N
30	Italy	ELDES- WR-10X		Epson Meteo	Milano	Backup				N	N
31	Italy	ELDES- WR-10X		Epson Meteo	Roma	2				N	N
32	Italy	ELDES- WR-10X		Regione Autonoma Trentino Alto Adige	Torbole	2				N	N
33	Italy	ELDES- WR-10X		UNIPARTHENOPE	Napoli	3				N	N
34	Netherlands	IDRA FMCW radar		Delft University of Technology	Cabauw tower	1	51,97	4,93	213	Y	Y
35	Poland	ELDES- WR-10X		Warsaw University	Warsaw	3				N	N
36	Swiss	-	-	Canton Wallis	Klein Matterhorn (Zermatt)	3	45,95	7,72	3883	N	N
37	Swiss	-	-	EPFL-LTE	Davos (temporary)	3	46,79	9,84	2152	Y	Y

Table 1 – X-band radar main characteristics (part 1)

ID	Country	Range (km)	D ant. (m)	Radome (Y/N)	h ant. (m)	Beam width (H)	Beam width (V)	Antenna Gain (dB)	Frequency (GHz)	Polarization tech.	Tx power (kW)	Pulse length (microsec)	MDS (dBm)	Starting date	Installation aim (i.e. Gap filling, urban hydrology)	Radar delivery cost (approx)	Annual Maintenance cost (approx)	Data availability (Y/N)	Contact (email)
1	Belgium	48	0.55 m hybrid array	Y		3.9 degr	10 degr. up/down	unkown	9410 +/- 30 MHz		4	0,8		2008	urban hydrology	53,8 Keuro	2,5 Keuro	N	johan.vanassel@aquafin.be
2	Denmark	60	fan-beam	N		0,95	20		9,41		25 (peak)	0,6		2010	Operational, urban hydrology, local forecast	102 kEuro			nej@dhigroup.com
3	Denmark	60	fan-beam	N		0,95	20		9,41		25 (peak)	0,6		2009	Operational, urban hydrology, local forecast	102 kEuro			nej@dhigroup.com
4	Denmark	60	fan-beam	N		0,95	20		9,41		25 (peak)	0,6		2009	Operational, urban hydrology, local forecast	102 kEuro			nej@dhigroup.com
5	Denmark	60	fan-beam	N		0,95	20		9,41		25 (peak)	0,6		2008	Operational, urban hydrology, local forecast	102 kEuro			nej@dhigroup.com
6	Denmark	60	fan-beam	N		0,95	20		9,41		25 (peak)	0,6		2009	Operational, urban hydrology, local forecast	102 kEuro			nej@dhigroup.com
7	Denmark	60	fan-beam	N		0,95	20		9,41		25 (peak)	0,6		2008	Operational, urban hydrology, local forecast	102 kEuro			nej@dhigroup.com
8	Denmark	60	fan-beam	N		0,95	20		9,41		25 (peak)	0,6		2009	Operational, urban hydrology, local forecast	102 kEuro			nej@dhigroup.com
9	France	50	0,60	Y	1,6	4	4	32	9,41		25	1,2	-92	2007	Local forecast			N	Meteo@eurocorps.org
10	France	100	1,80	Y		1,35	1,35	44,5	9,38	STAR Mode	>55	0.4-2.0	-112		Stationary			Y	Serge.Dalle@meteo.fr
11	France	100	1,80	Y		1,35	1,35	44,5	9,38	STAR Mode	>55	0.4-2.0	-112		Stationary			Y	Serge.Dalle@meteo.fr
12	France	100	1,80	Y		1,35	1,35	44,5	9,38	STAR Mode	>55	0.4-2.0	-112	2010	Stationary			Y	Serge.Dalle@meteo.fr
13	France	50	0,90	Y	1,6	2,5	2,5	37,5	9,41		25	1,2	-92	2007	Local forecast			N	patrick.thomas@meteo.fr
14	France	100	1,50	N		1,5	1,5	40	9,375		35	0,5-2,0			Gap filling / Alpine hydrology			N	jtestud@novimet.com
15	Germany	100	1,80	Y		1,35	1,35	44,5	9,38	STAR Mode	>55	0.4-2.0	-112	To be delivered	Aviation			N	frank.lehmickel@dwd.de
16	Germany	100	1,80	Y		1,35	1,35	44,5	9,38	STAR Mode	>55	0.4-2.0	-112	To be delivered	Aviation			N	frank.lehmickel@dwd.de
17	Germany	50	0,60	Y	16	4	4	32	9,41		25	1,0-2,0	-92	2009	Research			N	johannes.werhahn@kit.edu
18	Germany	50	0,90	Y	35	2,5	2,5	37,5	9,41		25	1,0-2,0	-92	2009	Research			N	h.bogena@fz-juelich.de
19	Germany	50	0,60	Y		4	4	32	9,41		25	1,0-2,0	-92	2009	Research			N	'corinna.rebmann@ufz.de'
20	Germany	50	1,20	Y	21	2	2	38,5	9,41		25	1,0-2,0	-92	2008	Internet publication			Y	huebener@klimagipfel.de
21	Greece	100	3,10	N		0,9	0,9	44	9,34		30	1,0		2005	Research				gram@env.meteo.gr
22	Italy	100	1,80	Y		1,35	1,35	44,5	9,375	STAR Mode	>55	0.4-2.0	-112	2008	Mobile	770 kEuro		Y	r.cremonini@arpa.piemonte.it
23	Italy	72	0,70	Y		3	3	35	9,41	NA	10 (peak)	0,6	>-105	2005					
24	Italy	100	1,80	Y		1,35	1,35	44,5	9,375	STAR Mode	>55	0.4-2.0	-112	2008	Aviation / volcanic ash detection			Restricted	g.vulpiani@protezionecivile.it
25	Italy	100	1,80	Y		1,35	1,35	44,5	9,375	STAR Mode	>55	0.4-2.0	-112	2008	Aviation / volcanic ash detection			Restricted	g.vulpiani@protezionecivile.it
26	Italy	100	1,80	Y		1,35	1,35	44,5	9,375	STAR Mode	>55	0.4-2.0	-112	2008	Aviation / volcanic ash detection			Restricted	g.vulpiani@protezionecivile.it
27	Italy	100	1,80	Y		1,35	1,35	44,5	9,375	STAR Mode	>55	0.4-2.0	-112	2008	Mobile			Restricted	g.vulpiani@protezionecivile.it
28	Italy	72	0,70	Y		3	3	35	9,41	NA	10 (peak)	0,6	>-105	2004					
29	Italy	72	0,70	Y		3	3	35	9,41	NA	10 (peak)	0,6	>-105	2009					
30	Italy	72	0,70	Y		3	3	35	9,41	NA	10 (peak)	0,6	>-105	2009					
31	Italy	72	0,70	Y		3	3	35	9,41	NA	10 (peak)	0,6	>-105	2009					
32	Italy	72	0,70	Y		3	3	35	9,41	NA	10 (peak)	0,6	>-105	To be installed					
33	Italy	72	0,70	Y		3	3	35	9,41	NA	10 (peak)	0,6	>-105	To be delivered					
34	Netherlands	Tx: H and V alternatelyRx: 2-channel receiver, H and V simultaneously	1.5, 15, 60		1,3	Y	1,8	1,8	38,65	9,475	1,2,5,10,20 W	0.02, 0.2	-103	2008	Research			Y	t.otto@tudelft.nl
35	Poland	72	0,70	Y		3	3	35	9,41	NA	10 (peak)	0,6	>-105	2010					
36	Swiss	60	fan-beam	N	7	0,95	20	n.d.	9,41	-	25 (peak)	0,7	n.d.	2007	Gap filling / Alpine hydrology	100 kEuro	1,5 kEuro	some	maurizio.savina@sfu.baug.ethz.ch
37	Swiss	~40	1,80	Y	~2	1,45	1,45	42,2	9,41	Simultaneous	7.9 per channel	variable	-74	2009	Research	500 kCHF	5 kCHF	not yet	alexis.berne@epfl.ch

Table 2 – X-band radar characteristics (part 2)